Shape Changing Airfoil

Eric A. Ott
General Electric Aircraft Engines, Cincinnati, Ohio

The NASA STI Program Office . . . in Profile

Since its founding, NASA has been dedicated to the advancement of aeronautics and space science. The NASA Scientific and Technical Information (STI) Program Office plays a key part in helping NASA maintain this important role.

The NASA STI Program Office is operated by Langley Research Center, the Lead Center for NASA's scientific and technical information. The NASA STI Program Office provides access to the NASA STI Database, the largest collection of aeronautical and space science STI in the world. The Program Office is also NASA's institutional mechanism for disseminating the results of its research and development activities. These results are published by NASA in the NASA STI Report Series, which includes the following report types:

- TECHNICAL PUBLICATION. Reports of completed research or a major significant phase of research that present the results of NASA programs and include extensive data or theoretical analysis. Includes compilations of significant scientific and technical data and information deemed to be of continuing reference value. NASA's counterpart of peer-reviewed formal professional papers but has less stringent limitations on manuscript length and extent of graphic presentations.

- TECHNICAL MEMORANDUM. Scientific and technical findings that are preliminary or of specialized interest, e.g., quick release reports, working papers, and bibliographies that contain minimal annotation. Does not contain extensive analysis.

- CONTRACTOR REPORT. Scientific and technical findings by NASA-sponsored contractors and grantees.

- CONFERENCE PUBLICATION. Collected papers from scientific and technical conferences, symposia, seminars, or other meetings sponsored or cosponsored by NASA.

- SPECIAL PUBLICATION. Scientific, technical, or historical information from NASA programs, projects, and missions, often concerned with subjects having substantial public interest.

- TECHNICAL TRANSLATION. English-language translations of foreign scientific and technical material pertinent to NASA's mission.

Specialized services that complement the STI Program Office's diverse offerings include creating custom thesauri, building customized databases, organizing and publishing research results . . . even providing videos.

For more information about the NASA STI Program Office, see the following:

- Access the NASA STI Program Home Page at *http://www.sti.nasa.gov*

- E-mail your question via the Internet to help@sti.nasa.gov

- Fax your question to the NASA Access Help Desk at 301–621–0134

- Telephone the NASA Access Help Desk at 301–621–0390

- Write to:
  NASA Access Help Desk
  NASA Center for AeroSpace Information
  7121 Standard Drive
  Hanover, MD 21076

Shape Changing Airfoil

Eric A. Ott
General Electric Aircraft Engines, Cincinnati, Ohio

National Aeronautics and
Space Administration

Glenn Research Center

October 2005

Contents

I. Shape Change Airfoil Project Introduction

A. Program and Project Background

The National Aeronautics and Space Administrations (NASA) Ultra Efficient Engine Technology (UEET) efforts have recently included the Intelligent Propulsion System Foundation Technology (IPSFT) Program. As part of the IPSFT Phase I (2003-2004) program, the Shape Changing Airfoil Project was established to investigate the utilization of intelligent control of airfoil shapes in order to reduce carbon dioxide emissions via reductions in engine fuel burn. Additional IPSFT project thrust areas in the Phase I effort included emissions, noise, and safety and reliability. Summaries of other projects focusing on these four major thrust areas, including a system study of the overall benefits of each of the IPSFT technologies are reported elsewhere.

The shape changing airfoil system was considered to be at technology readiness level (TRL) 1 as of the initiation of this Phase I effort. As a result, the Phase I project plan was structured to assess shape change concepts and form a technology foundation that could then be further proven and developed during the later phases of the program. In parallel to efforts to establish an intelligent control technology, the initial phases of the effort also were structured to begin establishing fundamental materials technology for higher strength, intermediate temperature aluminum alloys which were envisioned to be candidates for a the backbone structure of a lightweight, affordable, shape changing airfoil system. The advanced aluminum material was intended to be a future base metal for the airfoil upon which the control system and related actuation materials and structures could be added. Performance of the shape change concept study and advanced aluminum alloy technology development efforts concurrently was intended to allow sufficient time for both technology areas to reach TRL 6 by 2009. Fundamental material and process models were also being addressed in this project in order to accelerate the insertion of new materials technology. The GE Aircraft Engines engine system being considered as a baseline for assessment of the intelligent engine technologies is the 2015 Quiet Aircraft Technology (QAT). The QAT utilizes a commercial engine cycle with a number of advanced engine technologies studied under other GE Aircraft Engines contract efforts.

This Shape Changing Airfoil project effort was designed around a General Electric (GE), NASA and Ohio State University (OSU) collaboration arrangement. Separate contracts were placed by NASA with GE and OSU, but efforts were performed in a collaborative fashion in order to best utilize the personnel, experience, analysis, and testing strengths of each of the collaborating organizations. The project areas covered in this final report relate specifically to the GE portion of the Shape Changing Airfoil effort; however, appropriate references to results achieved as part of the OSU investigation under this project focus area are included. Additional details can be found in the OSU final report to be published at the conclusion of the OSU Phase I efforts. The aluminum development efforts and the shape change concepts development portions of this project will be summarized in Sections II and III respectively.

B. Project Objectives

The overall objective of this project was to develop materials and computational models to enable the design and fabrication of lightweight, high-strength shape-changing airfoils. The emissions improvement goal associated with this technology area was a 0.5% specific fuel consumption reduction. Such reductions would result in significant carbon dioxide emission reductions. Specific fuel consumption reductions were investigated through the study of shape change concepts in airfoil-type components and through development of lightweight airfoil materials fundamentals.

C. Project Team and Plan

Efforts performed in this project were organized into 4 separate subtasks. A summary of the Phase I subtask objectives are given in Figure 1.3.1. Subtasks 1 through 3 were performed as a collaboration between GE Aircraft Engines, GE Global Research, Transmet Corporation, and Ohio State University, with NASA Glenn Research Center in an advisory role. Subtask 4 was performed as a collaboration between GE Aircraft Engines, and GE Global Research Center, again with NASA Glenn Research Center in an advisory role. A more detailed project plan and schedule can be found in Section VI. A summary of the core project team and team member affiliations is given in Table 1.3.1. Additional personnel were also consulted during this effort for guidance during various technical activities.

Phase I Shape Changing Airfoil Project Structure
    Subtask 3.2.1: Nano Phase Aluminum Alloying Concepts
- *"Select most promising aluminum alloy compositions for evaluation as lightweight, high-strength shape changing materials."*
- *"Manufacture lab-scale dispersion-strengthened aluminum alloys by rapid solidification techniques."*

    Subtask 3.2.2: Nano Phase Aluminum Processing and Characterization
- *"Identify lab-scale manufacturing techniques for nano-phase aluminum materials."*

    Subtask 3.2.3: Nano Phase Aluminum Modeling
- *"Nano Phase Aluminum Modeling"*

    Subtask 3.2.4: Shape Change Technology Scoping
- *"Perform aerodynamic analyses to determine blade shape change requirements and potential benefits."*
- *"Assess shape changing materials technologies."*

Initial Phase 2 Shape Changing Airfoil Project Plans
- Develop, produce and test lab-scale nano-phase aluminum materials using candidate manufacturing techniques selected in Phase 1.
- Conduct manufacturing scale-up studies.
- Develop and produce nano-phase aluminum for high-strength lightweight blades.
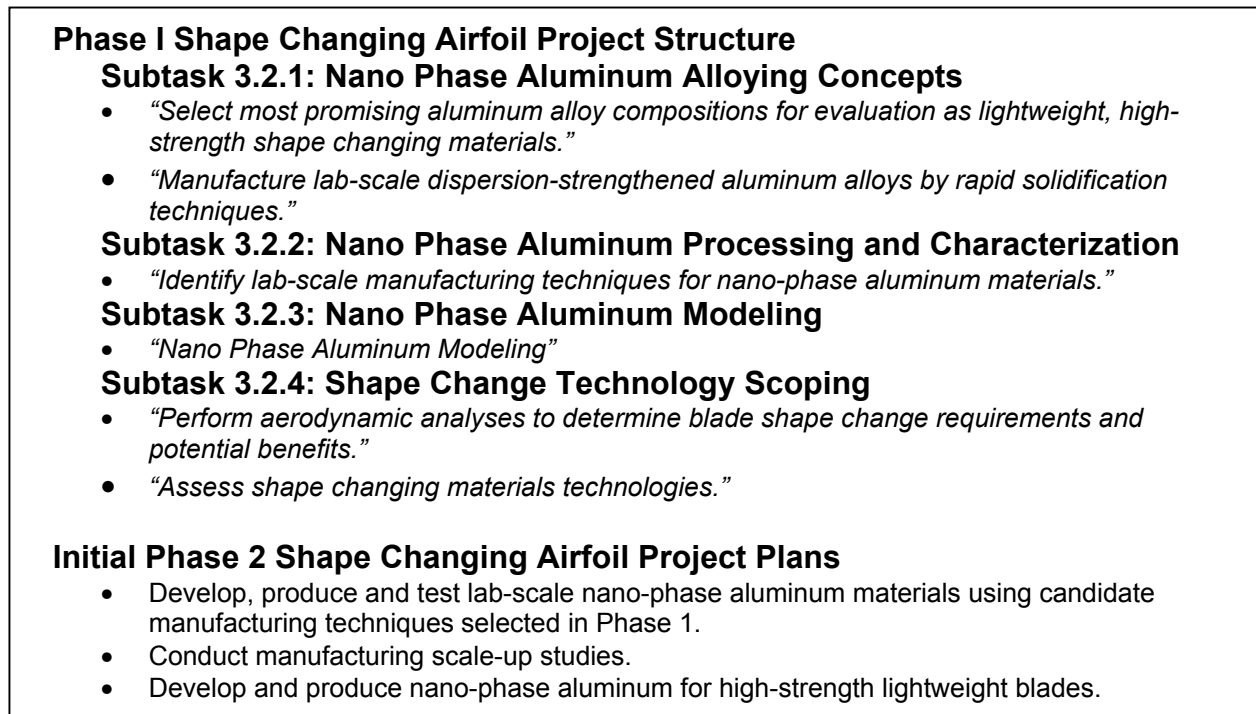

Figure 1.3.1: Outline of the Shape Changing Airfoil Project Effort Phases I and II.

Table 1.3.1: Summary of Shape Changing Airfoil Project Team

Organization	Team members	Relevant Tasks (3.2.x)
GE Aircraft Engines	Eric Ott (Lead)	1,2,3,4
	John Decker	4
GE Global Research Center	Shyh-Chin Huang	1,2,3
	Don Lipkin	4
	Matthew Lear	4
NASA Glenn Research	Robert Draper (Monitor)	1,2,3,4
	Ronald Noebe	1,2,3,4
Ohio State University	Michael Mills	1,2,3
	Glenn Daehn	1,2,3
	Mark Carroll	1,2,3
Transmet Corporation	Doug Shull	1,2,3
	Bruce Rademan	1,2,3

D. Deliverables

The project effort deliverables for Phase I are given below. The present report specifically addresses interim report requirements in the first 3 deliverables. For the fourth deliverable, material samples were produced and submitted to OSU for characterization as part of the project plan and as such this deliverable was also completed.

1. Interim report on blade shape change requirements and benefits.
2. Interim report on shape changing materials technologies, including most promising aluminum alloy compositions.
3. Interim report on lab-scale manufacturing techniques for nano-phase aluminum materials.
4. Dispersion-strengthened aluminum alloy sample.

II. Technical Summary of Aluminum Alloying Fundamentals Tasks

Aluminum material development efforts included identification of approaches, production of materials, processing and characterization of alloys, and modeling of strengthening. These efforts were intended to provide a base of simple alloying concepts from which more complicated alloy compositions and microstructures may be developed in later phases of this effort. Tasks were performed by GE, Transmet Corporation (a subcontractor to GE), and OSU. Material identification, generation, and consolidation efforts were led by GE while characterization and modeling efforts were led by OSU.

The overall alloying approach chosen in this study was based on the use of rapid solidification (RS) processing in order to develop high strength, highly stable alloys and microstructures. Many of the material structures which develop out of RS processing have microstructural features which are on the nanometer size scale and as such the alloys are also referred to as "nano" aluminum in this study. The use of RS processing and the resulting "nano" aluminum alloys was expected to provide the material strengthening

mechanisms whereby significantly improved strength levels and temperature capability could be achieved relative to conventionally processed aluminum alloys.

Application requirements driving the "nano" aluminum developments were established based on large diameter commercial engine fan blade applications. Other airfoils, both rotating and stationary, may also benefit from successful development of this technology, although the specific property requirements may differ. Conventional fan blade materials typically include polymer matrix composites, or titanium. The choice in materials is often driven by diameters. Hollow titanium blades have also been used by some engine manufacturers. Other rotor and stator airfoils are frequently composed of titanium, aluminum, or polymer matrix composites. Operating conditions for large diameter commercial fan blade applications require high strength, fatigue resistance, ductility, erosion and impact tolerance, thermal stability, and environmental resistance. Such parts are considered critical to the operation and safety of the engine. Relative to conventional fan blade material choices, the aluminum material system being developed in this study was intended to be lighter in weight compared to titanium and lower in complexity and cost relative to a polymer matrix composite. Alloy development efforts were driven primarily by the need for improvements in ambient and elevated temperature yield strength, maintaining substantial ductility for impact tolerance, and ensuring microstructure stability to intermediate temperatures. Specific property goals used to guide Phase I aluminum alloy foundation development efforts were:
1) ambient temperature strength levels of 90ksi (610Mpa),
2) ambient temperature ductility of at least 5%,
3) strength at 280°F (140°C) of 60ksi (410Mpa), and
4) thermal stability to 300°F (150°C).

These requirements were established to guide selection of general strengthening approaches and candidate alloy systems. Significantly more detailed property requirements would need to be assessed in subsequent phases of the project when simple alloying and strengthening concepts are to be combined into more complicated candidate alloy systems.

A. Subtask 3.2.1: Nano Phase Aluminum Alloying Concepts

Efforts in this task involved the selection of basic aluminum alloy compositions for study of alloying approaches, investigation of techniques to introduce dispersoids within a rapidly solidified aluminum alloy matrix, as well as generation of rapidly solidified materials to be consolidated and characterized in Task 3.2.2. Work was performed by GE Aircraft Engines and GE Corporate Research and, through GE subcontract, by Transmet Corporation. Final alloy composition selections were discussed and agreed upon by the project team including NASA, GE, OSU, and Transmet Corporation.

Alloy and Alloying Technique Selection

There are two commercial alloy series specifically developed to achieve high strength, but neither can maintain high strength in the temperature range from room temperature to

300ºF, as required by the present application. One is the 7xxx-series of alloys which derive their strength from fine GP-zone precipitation of a semi-coherent Zn_2Cu phase. The 7xxx-series of "high strength" alloys approach the ambient temperature strength requirements of the present application, but their strength falls off sharply with temperature and is not unacceptable above 250ºF. Temperature capability limits are typically attributed to precipitate coarsening and subsequent loss of strength with time at elevated temperatures. The 2xxx-series of aluminum alloys have been developed to maintain strength to temperatures above 450ºF. This series of "high temperature" alloys derive their strength mainly from solid solution strengthening via Cu addition. Although GP-zone precipitation can also be formed to provide additional strengthening, the strength of the 2xxx-series alloys is significantly lower than target requirements in this effort for both ambient and 300ºF temperatures. These trends and the project tensile requirements are shown in Figure 2.1.1
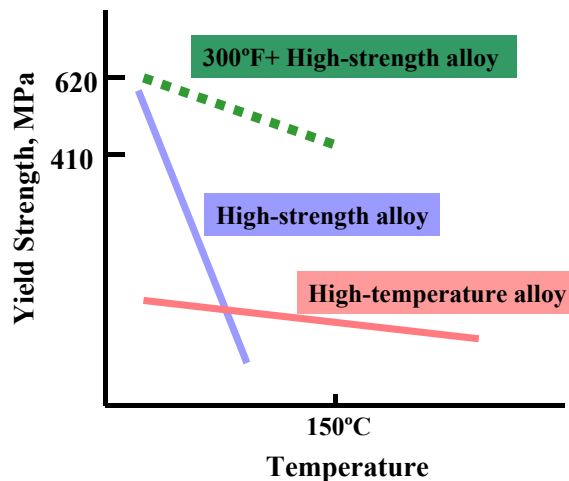

Figure 2.1.1: Aluminum alloy tensile property goals relative to conventional alloys.

New alloying and strengthening approached are necessary to achieve high strength over the temperature range from room temperature to 300ºF. The conventional precipitation strengthened alloying approaches utilized in alloys such as 7xxx- and 2xxx-type aluminums will have to be abandoned or supplemented by new strengthening approaches, Figure 2.1.2. New alloy composition domains will also need to be explored to take advantage of the benefits of novel processing routes such as RS processing.

Several new alloying concepts were formulated and led to the development of the Phase I plan. The primary concept was based on dispersion strengthening with nano-scale particles using rapid solidification processing techniques. Due to the thermal stability requirement, it was necessary to pursue dispersion phases which were highly stable including those which may be formed from liquid state during solidification. Rapid-solidification processing was used to produce nano-scaled particle dispersions with sufficient volume fractions and spacings to be effective strengtheners. In one approach, an oxide dispersion was considered, due to the increased availability of nano-sized oxide powder recently and the identification of a possible low-cost process that could incorporate

the nano particles into aluminum. In a second approach, two classes of dispersion phases formed by precipitation, icosahedral and L1$_2$, were pursued due to their desirable thermal stability and ability to respond to rapid-solidification to produce fine dispersions of particles. At a later stage in the evaluation effort, interesting aspects of the Al$_6$Mn dispersion phase were observed in this program, and the Al-Mn system was subsequently pursued in place of the oxide dispersion approach. These concepts are described in additional detail in the subsequent paragraphs as are a few candidate alloying approaches which were not selected for pursuit in this project.

Figure 2.1.2: Schematic showing several candidate aluminum alloying approaches.

Oxide dispersion in a 2219 matrix

Stable oxide dispersions are used in several conventional mechanically alloyed nickel- and iron-based alloys in order to provide elevated temperature strengthening. Matrix strengthening is provided by a combination of solid solution and/or precipitate strengthening via alloying and dispersion strengthening by the introduction of fine ceramic particles in such structures. Reliable introduction of a fine oxide dispersion is complicated by several factors including density differences between the dispersoid compound and the matrix, high interfacial energies, and complicated solidification processes. Many existing oxide dispersion strengthened alloys are manufactured by powder metallurgy approaches involving extensive ball milling to introduce a fine oxide throughout the metallic matrix. Such processing is difficult and costly. In highly ductile alloy systems, low temperature milling may be required to be effective.

An alternate approach was identified by GE whereby fine oxide powder could be introduced into molten aluminum in a way that promoted formation of a uniform particle distribution in solidified product. This technique utilized the spinning cup process practiced by Transmet Corporation. Such dispersions were expected to provide excellent thermal stability and improved strength. The commercial 2219 alloy was chosen as a base metal matrix for convenience and Al$_2$O$_3$ was selected as selected as the dispersoid. The target Al$_2$O$_3$ size range was 20nm or less to enable fine particle spacings while maintaining the

ceramic volume fraction as low as possible to minimize any adverse impact to ductility. A relationship between particle size, volume fraction, and anticipated Orowan-type [1] strengthening increment is given in Figure 2.1.3.
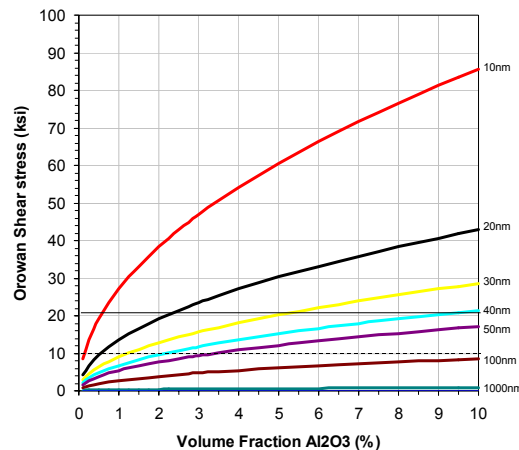

Figure 2.1.3: Estimation showing the approximate Orowan [1] relationship between dispersoid distribution and potential strengthening benefit assuming non-shearable particles.

Icosahedral phase dispersion

The icosahedral phase was first discovered in aluminum alloys in the 1970's. It is a metastable phase formed by solidification due to the slow diffusivity of certain alloying elements such Fe, Ni and Co [2]. It has a complex crystalline structure with 20 faces, which can only grow to form "quasicrystals" with cavities, as shown in Figure 2.1.4. Due to the loosely packed structure, quasicrystals are known to be effective strengthening particles. Furthermore, a large volume fraction (>20%) of fine (<200μm) icosahedral phase particles can be produced by rapid solidification processing. A first icosahedral-phase strengthened aluminum alloy, nominally Al-7Fe-1.5V-1.5Si [3], was developed by Allied-Signal in the 1980's with good combination of strength, temperature capability, fatigue and corrosion resistance.

Tohoku University of Japan has also investigated additional icosahedral phase alloys [4] in the 1990's. Several new icosahedral phase systems were identified with attractive combinations of ductility and strength. One of the alloys studied extensively by the Tohoku University group was $Al_{93}Fe_3Cr_2Ti_2$ [5]. Figure 2.1.5 shows the yield strength of this alloy as a function of testing temperature (data labeled Al-Fe-Ti-Cr alloys). As seen, the strength of this icosahedral alloy system is equivalent to that of the 7xxx-series alloy at room temperature, but it strengths maintained over a much larger temperature range more similar to that of high temperature 2xxx-series alloys. This icosahedral alloy system thus shows the potential of meeting the program goals, and was selected for investigation here.
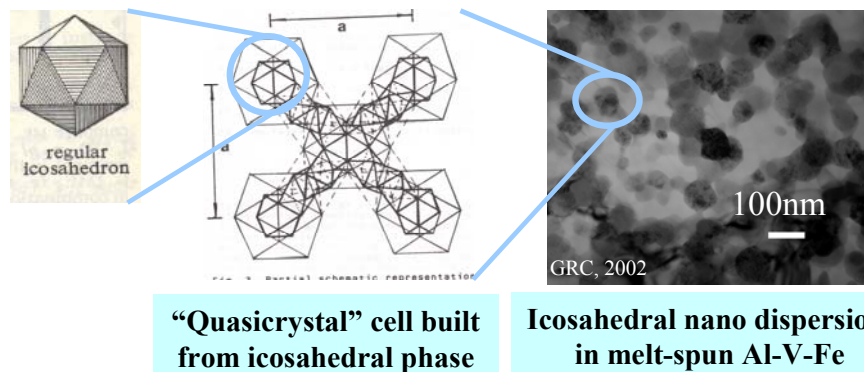
Figure 2.1.4: Icosohedral phase structure schematic [2] and an example transmission electron micrograph from previous GE studies.
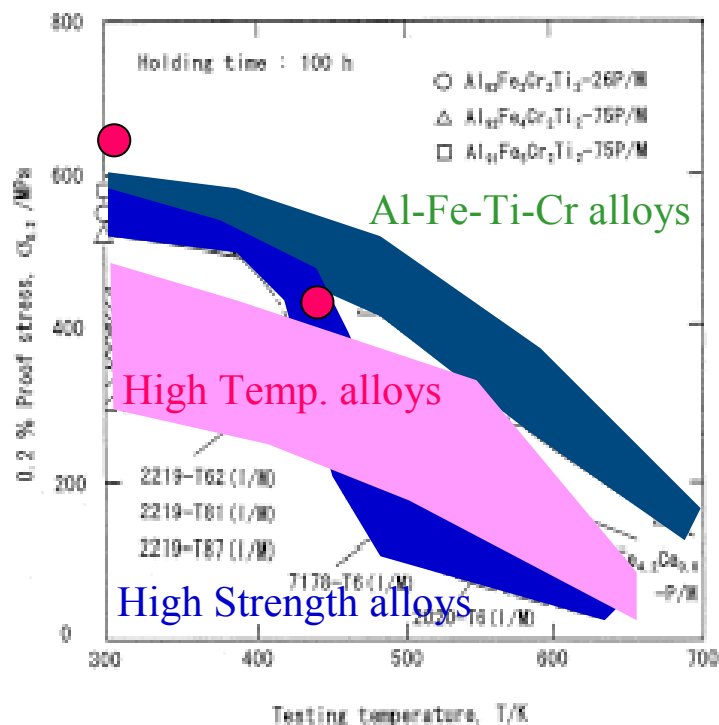

Figure 2.1.5: $Al_{93}Fe_3Cr_2Ti_2$ properties as reported by Inoue, et al. [5] compared to conventional high temperature alloys and project strength requirements (red circles).

$L1_2$ phase dispersion

As in the case of Ni_3Al strengthening in Ni-based superalloys, $L1_2$ phases have been identified in aluminum alloys. Several of these phases and their potential strengthening benefits have been reported in the literature, for example, Al_3Li, Al_3Zr and Al_3Sc. The most successful strengthening phase was Al_3Sc [6]. By powder metallurgy processing techniques, alloys containing as little as 0.3 wt.% Sc have been shown to exhibit strength

levels greater than 500MPa. Unlike Al_3Li, however, the Al_3Sc phase can form by rapid solidification or by high temperature annealing above about 575ºF (300ºC). The Al_3Sc $L1_2$ phase, as well as the similar Al_3Zr phase have the potential of providing high strength up to temperatures in the 300ºF (150ºC) range. A drawback for the Al_3Sc dispersion approach is the cost impact to the alloy from the current Sc elemental cost. Sc costs in the range of 3 or more orders of magnitude greater than that of Al are prohibitive. Even with just a few tenths of a percent addition, it can increase the material cost significantly. In this program, an alloy composition was formulated based on 0.15 wt.% additions of Sc and Zr to the icosahedral phase alloy $Al_{93}Fe_3Cr_2Ti_2$ identified above.

Al_6Mn dispersion alloys

Based on characterization results obtained from the 2219+ Al_2O_3 dispersion alloy efforts in this study, a fine dispersion of the Al_6Mn phase was identified at low Mn levels. The project team agreed to produce a several Al-Mn binary alloy with three Mn contents to enable more detailed understanding of the strengthening effects of the Al_6Mn dispersion. A phase diagram [7] for the Al-Mn system showing the limited Mn solubility in pure aluminum and the stability of the Al_6Mn phase to temperatures above the melting point of pure aluminum is given in Figure 2.1.6.
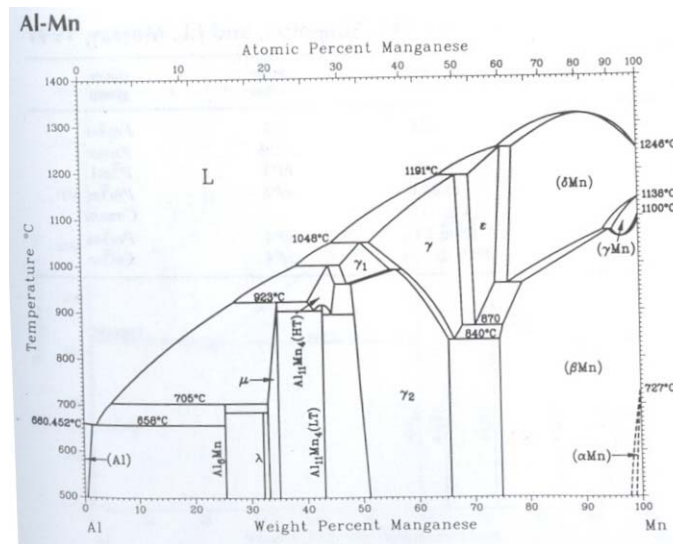

Figure 2.1.6: Al-Mn binary phase diagram [7] showing limited Mn solubility and high thermal stability of the Al_6Mn phase.

Final Phase I Alloy Selection

Technical assessment of candidate aluminum alloy compositions was performed and six alloy compositions were selected for manufacturing by rapid solidification processing in this

project. All alloys, with the exception of two additional conventional baseline alloy compositions from alloys 7075 and 2219, were chosen such that fine dispersions of strengthening particles could be produced within the matrix. Two primary dispersoid-producing approaches were used – introduction of fine, stable Al_2O_3 into a molten aluminum matrix followed by RS processing and formation of highly stable precipitates from a super-saturated matrix during solidification, cooling, or subsequent aging after rapid solidification processing.   A summary of nominal alloy compositions targeted is given in Table 2.1.1 below.

Table 2.1.1: Selected alloy nominal target compositions (wt.%) used for dispersoid alloys.

Alloy	Al	Ti	Cr	Fe	Sc	Zr	other
Icosahedral	Bal.	2	2	3	-	-	-
Icosahedral+Sc,Zr	Bal.	2	2	3	0.1	0.2	-
2219-Al2O3	Bal.	-	-	-	-	-	Al-2219 matrix
Al-1Mn	Bal.	-	-	-	-	-	1%Mn
Al-1.5Mn	Bal.	-	-	-	-	-	1.5%Mn
Al-2Mn	Bal.	-	-	-	-	-	2%Mn

(a)   (b)

Figure 2.1.7: Transmet rapid solidification processing showing (a) melt spinning of flake, and (b) centrifugal atomization (Courtesy of Transmet Corporation).
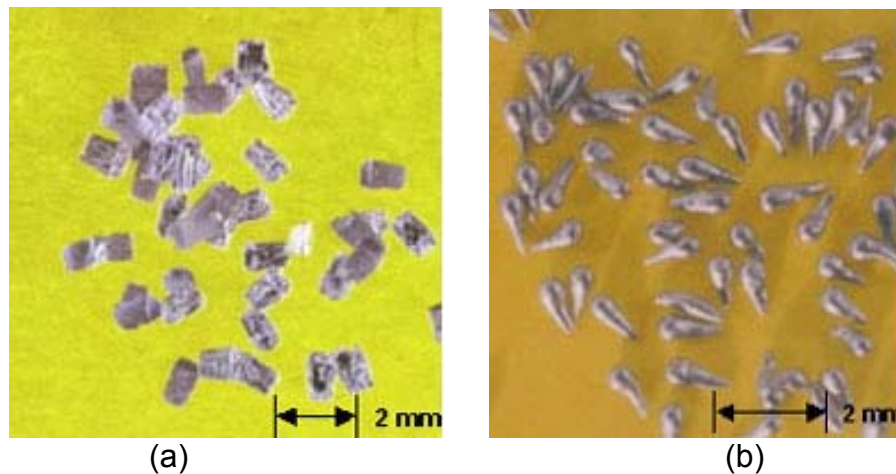
(a)   (b)

Figure 2.1.8: Typical particulate materials resulting from (a) melt spinning of flake, and (b) centrifugal atomization (Courtesy of Transmet Corporation).

Table 2.1.2: Nominal and measured alloy compositions (wt.%)

Alloy	Chem.	Al	Ti	Cr	Fe	Sc	Zr	Mn	other
7075 baseline	Bar*	86.6	-	0.21	0.14	-	0.013	0.023	6.3Zn, 1.85Cu, 2.58Mg, 0.25Si
2219 baseline	Bar*	93	-	-	0.046	-	0.12	0.27	6.43Cu, 0.046Si, 0.089V
Icosahedral	Nom.	Bal.	2	2	3	-	-		-
	Casting**	Bal.	1.92	1.70	3.05	-	-	-	0.03Cu, 0.09Si
Icosahedral +Sc,Zr	Nom.	Bal.	2	2	3	0.1	0.2		-
	Casting**	Bal.	1.82	1.80	2.82	0.1	0.13	-	0.05Cu, 0.08Si
Al-1Mn	Nom.	Bal.	-	-	-	-	-	1	-
	Casting***	98.8	-	-	0.038	-	-	1.05	0.035Si
Al-1.5Mn	Nom.	Bal.	-	-	-	-	-	1.5	-
	Casting***	98.4	-	-	0.042	-	-	1.50	0.035Si
Al-2Mn	Nom.	Bal.	-	-	-	-	-	2	-
	Casting***	97.8	-	-	0.042	-	-	2.03	0.036Si

* Input bar stock subsequently melted for flake generation
** Pre-alloyed cast plates subsequently melted for flake generation
*** Cast sample taken from melt during flake generation process.

Phase I Rapid Solidification Processing

Two rapid solidification processing (RSP) methods – centrifugal atomization and melt spinning were selected for generation of material in this study. Both RSP methods, shown in Figure 2.1.7, have been previously scaled-up to production by Transmet, although sub-scale equipment was used for this study. Typical particulate material morphologies generated by these processes are given in Figure 2.1.8. The oxide dispersion alloy was generated using a centrifugal atomization, spinning crucible technique. Solidified material

was collected as particulate or was splat quenched on a substrate for characterization and analysis. Flake materials from the remaining baseline and experimental alloys were generated by melt spinning using pre-alloyed bar or cast plates of the target composition. Materials for the 7075 baseline, icosahedral and Al-Mn alloys were provided to the program by GE. For the Al-Mn binary alloys, a single master alloy with 2% Mn was generated and was subsequently diluted with pure Al to generate lower Mn content materials. The pure aluminum material was chosen to best match the Al-2%Mn master alloy impurity levels to enable a direct comparison of Mn compositions. All flake materials were generated in an ambient environment melt spinning apparatus at Transmet Corporation. As-produced flake was shipped to OSU for analysis of the as-produced structure and to GE Global Research for canning and extrusion consolidation. Additional cast buttons of the Al-Mn alloys were also produced to enable comparison of phase morphologies in the as-cast condition to that of rapid solidification processed material. Actual measured chemistries are given in Table 2.1.2 along with nominal compositions for reference.

Process development trials for introduction of a fine Al_2O_3 ceramic dispersoid into a rapidly solidified aluminum were performed by Transmet Corp. where trial runs, 3-5 pounds each, were converted to splat quenched and particulate material for subsequent evaluation. A total of more than 20 development trials were performed. Characterization activities in Subtask 3.2.2 concluded that the process used for introduction of Al_2O_3 ceramic particles was not fully successful and a decision was made to abandon pursuit of the 2219-Al_2O_3 dispersoid alloy. Results did, however, suggest that an alternate approach could be used to produce a dispersion of Al_6Mn. The Team decided to replace the 2219-Al_2O_3 dispersoid alloy with three experimental Al-Mn binary alloy compositions.

B. Subtask 3.2.2: Nano Phase Aluminum Processing and Characterization

This task is composed of several subtasks which were shared by GE and OSU. GE assessed and performed consolidation of rapidly solidified material produced in Task 3.2.1 to generate bulk materials for characterization and evaluation by OSU. A schematic summary of the process is given in Figure 2.2.1. The OSU characterization efforts included defining characterization techniques, assessing as-produced material, and performance of a heat treat and exposure study to understand microstructural evolution with time and temperature. Additional alloy consolidation efforts were also undertaken by OSU in order to generate additional material for analysis from flake. A more detailed summary of the OSU characterization efforts can be found in the OSU final report to be published following completion of the Phase I OSU effort.
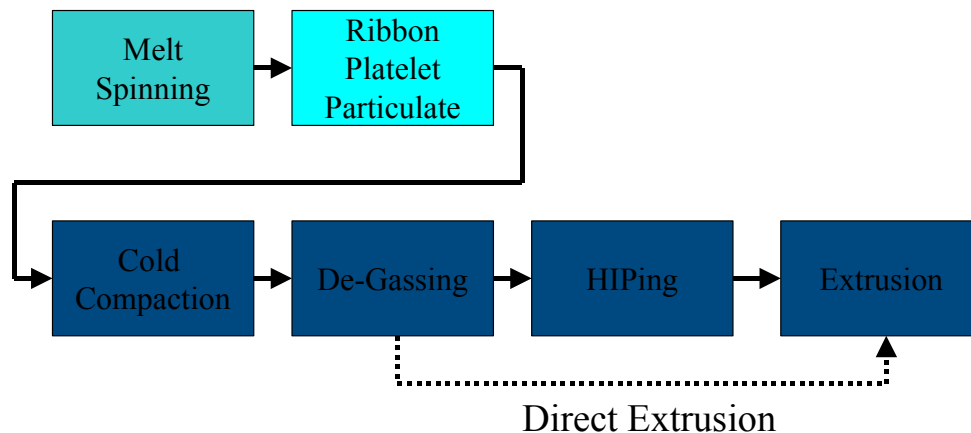
Figure 2.2.1: Schematic of the aluminum alloy consolidation processing method.

Consolidation processing to produce bulk nano-phase aluminum materials

Two consolidation methods were used depending upon RSP type. For the 2219-Al_2O_3 alloy, a production-type system was modified so that molten droplets could be collected prior to their solidification into powder, as well as collection of particular material. Molten droplets were collected on a substrate material and built up to thicknesses on the order of about 0.25 inches (0.5mm). So called, splat quenched material was investigated in the as-produced form and to reduce inherent as-produced porosity, after direct rolling. Melt-spun flake materials were consolidated by extrusion into bulk material. To preserve the nano-phase structure in the bulk material, a low temperature processing was necessary. Furthermore, flake materials display large flat surfaces and a thermomechanical process is preferred to minimize prior-particle boundary defects in the consolidated material. Shear deformation occurring during extrusion was expected to provide more consistent consolidation of flake compared to simple hot isostatic press (HIP).

<u>*Oxide dispersion strengthened 2219 aluminum consolidation*</u>

Runs included in the centrifugal atomization DOE were generated in particulate and/or bulk form for analysis. The bulk, splat quenched material form was considered to be the most convenient for characterization efforts. A view of a typical splat quenched material run output is given in Figure 2.2.2. Efforts were discontinued on this material system and dispersion production method due to difficulties in producing a uniform distribution of ceramic particles in the aluminum alloy matrix with the spinning conditions utilized. Additional development effort would be required in order to improve the reliability of this process and the uniformity of the dispersion type alloy produced.

Figure 2.2.2: Typical view of a splat quenched 2219 + Al_2O_3 alloy.

Extrusion of baseline 7075 flake material

Consolidation of 7075 melt spun flake material was performed by containered extrusion at elevated temperature with care exercised in removing absorbed H_2O absorbed on the surfaces of the flake material. The final dimensions of the extruded rod was about 7/8" diameter by 110" long, as shown in Fig. 2.2.3. A section from the middle of the extruded rod was cut and polished. It showed sound consolidation without any signs hydrogen contamination, as also shown in Figure 2.2.3 (top right). The extruded material was then sent to Ohio State University for further characterization. As a result of the success of the first, and more difficult of the two baseline alloys in the extrusion process, the consolidation design of experiments (DOE) was discontinued in favor of providing additional resources for extrude consolidation of Subtask 3.2.1 RSP dispersoid alloy flakes.

Figure 2.2.3: Photograph of the 7075 baseline alloy extrusion and (top right) a cross section indicating no gross porosity.

Extrusion of 2219, icosahedral phase and Al-Mn alloys

The extrusion procedure used for the alloy 7075 baseline material was also used for additional flake alloys, but the extrusion can was redesigned to accommodate processing of smaller quantities of multiple flake alloy materials. The extrusion runs were focused on consolidation of the 2219 baseline material, the two icosahedral alloys, and the three Al-Mn alloys to small diameter bar for OSU characterization efforts and limited mechanical testing. To obtain the small diameter, the extrusion can was redesigned to allow a group of three alloys to be co-extruded.

Extrusion of both the icosohedral/2219 set and the Al-Mn set resulted in difficulties with applying sufficient press ram force to effectively extrude the can and aluminum flake materials through the extrusion die. A very limited amount of the Al-Mn alloy extrusion was successfully extruded prior to reaching the maximum press capacity. Further extrusion efforts were discontinued in lieu of alternate processing identified by OSU. A macro photograph of the short extrusion section containing three Al-Mn alloys and the remainder of the extrusion can that could not be successfully processed is given in Figure 2.2.4.

Figure 2.2.4: Photographs of the unsuccessful Al-Mn extrusion at the can side (left) and at the extruded side (right) after removal from the extrusion die.

Al Alloy Characterization

Characterization efforts were performed by OSU and will be summarized in detail in the OSU final report. Efforts are not yet complete as of the writing of this final report since the end of the Phase I OSU effort extends beyond that of GE. The characterization performed to date clearly indicates the value of using RS processing to convert eutectic-like microstructure morphologies to more finely dispersed particles which are, in turn, expected to provide significant matrix strengthening. Fine grain structures are apparent in as-produced RSP materials and there is evidence that relatively fine structures are maintained through subsequent thermal processing.

Analysis of the 2219+ Al_2O_3 alloy splat quenched samples, shown in Figure 2.2.5(a-c), indicated that Al_2O_3 particles were not distributed uniformly at a fine (<1um) size scale by the processing. More detailed analysis of the Al_2O_3 source powder confirmed that particle

sizes were significantly larger than that originally targeted. Characterization results, however, still suggest that the particle introduction technique parameters were not sufficient to form a uniform particle distribution. Also, due to the relatively slow cooling rate of molten material during splat quench, residual eutectic structures from the 2219 alloyl constituents can also be seen. Transmission electron microscope (TEM) analysis, however, did point out an unanticipated benefit. Even at relatively low Mn contents (0.3% in this case) a fine dispersion of particles consistent with the Al_6Mn phase can be formed after RS processing and subsequent high temperature aging heat treatment.

(a)

(b)

(c)

(d)

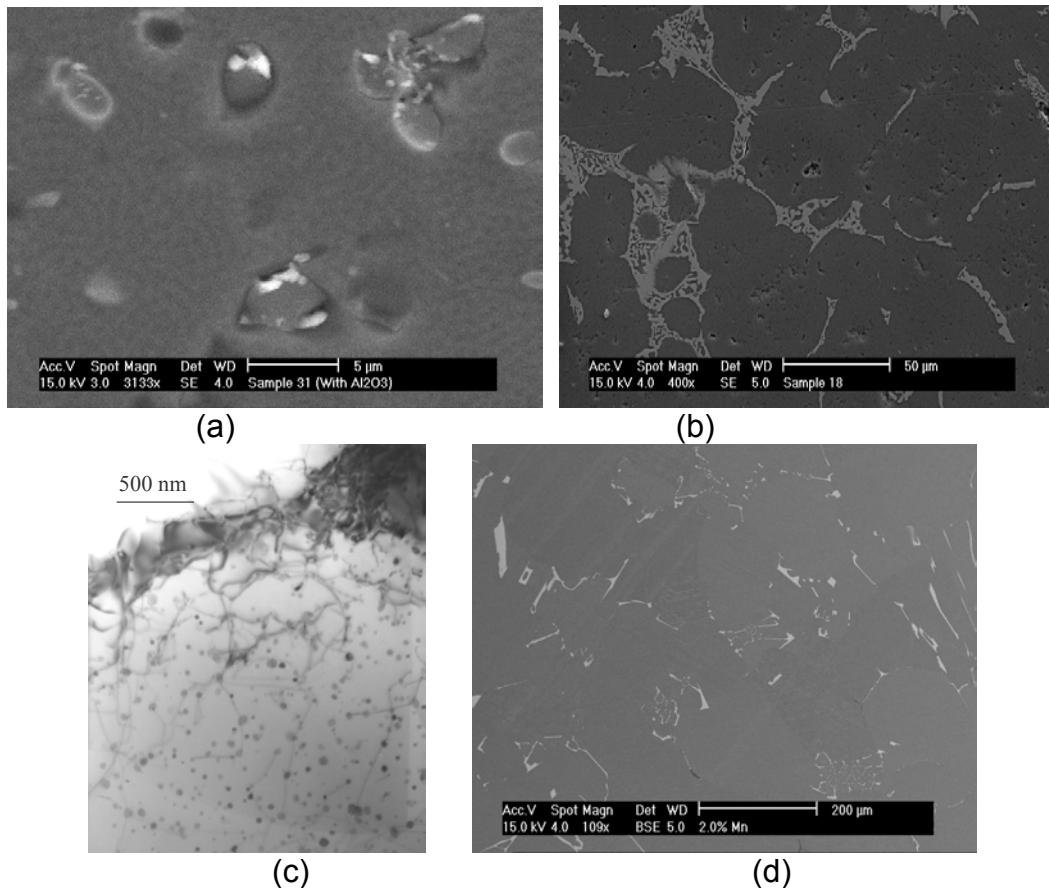Figure 2.2.5: 2219+ Al_2O_3 produced by centrifugal atomization and splat quenching showing (a) non-optimum distribution of ceramic (bright contrasting phase), (b) typical eutectic structures in 2219 base metal, (c) presence of fine Al_6Mn in splat quenched and heat treated material, and (d) a microstructural comparison to a similar Al-Mn alloy produced at slower cooling rates as a cast button.
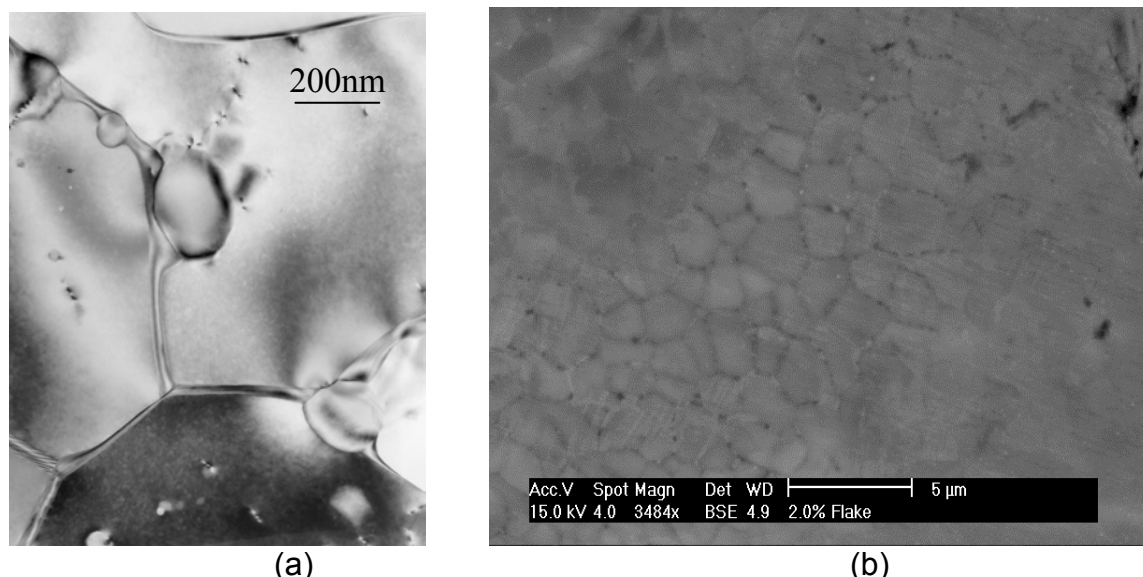
<center>(a)</center>

<center>(b)</center>

Figure 2.2.6: Al-Mn binary alloy characterization analysis performed by OSU showing (a) Al6Mn particles pinning grain boundaries and (b) ultra-fine grain structures.

In the Al-Mn binary alloys, it was found via characterization efforts that the Al_6Mn particles are present in the microstructure and appear to act in several beneficial capacities – pinning grain boundaries to enable ultrafine, as-produced grain structures (Figure 2.2.6), fine dispersoids which are stable to >750°F(400°C) and which show interaction with dislocations as suggested by Orowan-type mechanisms. Examples are shown in Figure 2.2.7. Fine grain structures are also stable at temperatures as high at 750°F(400°C).

Characterization efforts being performed by Ohio State University (OSU) have indicated that as-produced alloy flake materials display very fine grain sizes in the range of about 0.1-1 micrometer in size and selected thermal processing can be used to produce fine precipitate dispersions in these materials. Comparison of the melt spun Al-Mn materials to the cast Al-Mn buttons produced by Transmet as part of this project indicated that melt spinning is beneficial in limiting the formation of coarse second phase eutectic structures in highly alloy compositions. OSU characterization efforts continue on as-produced flake materials, consolidated bulk materials, and similar materials after heat-treat processing.
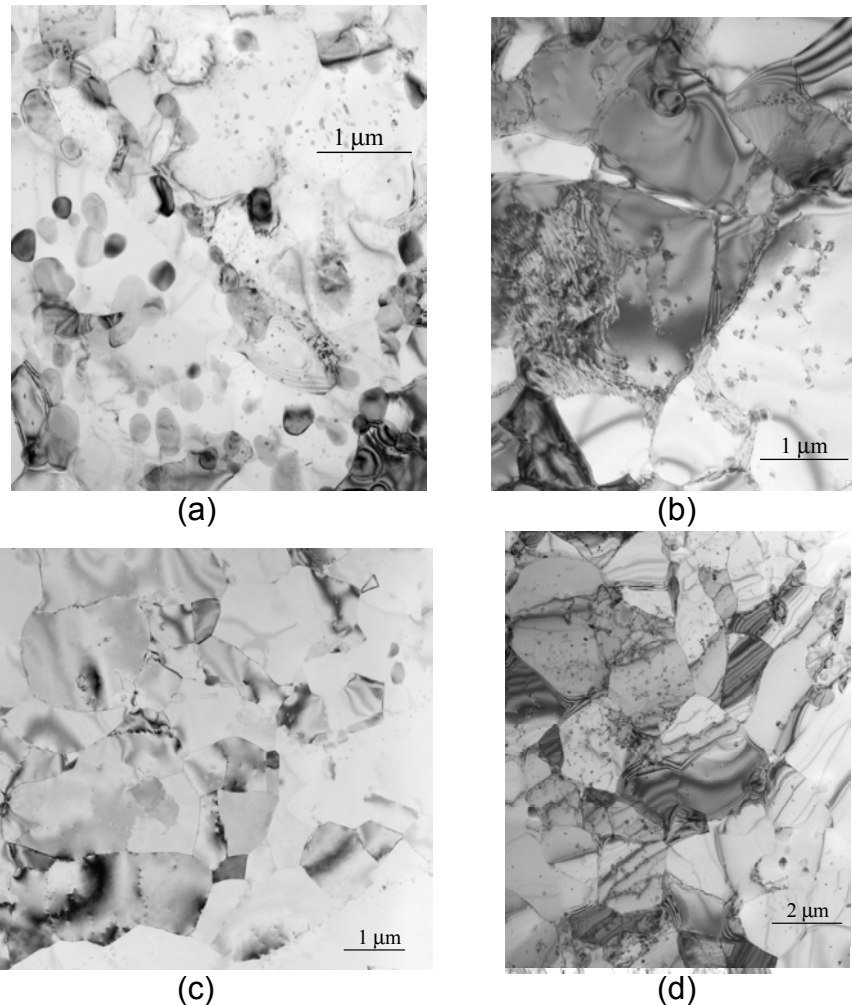
Figure 2.2.7: Al-Mn binary alloy 750°F(400°C) exposure effects showing (a) a bimodal Al$_6$Mn distribution, (b) effective dislocation particle interaction, (c) a fine micron or sub micron grain size, and (d) stability of the fine structure at 750°F(400°C) for 27 hrs.

C. Subtask 3.2.3 Modeling

This task is being performed by Ohio State University under contract directly from NASA. GE participation in this task is primarily in providing material generated in other tasks, consulting with OSU on technical scope and details, and reviewing results. The OSU generated model and early analysis of several baseline and Al-Mn alloy compositions suggest that significant strength improvements are attainable with an Al-Mn alloy having a fine dispersion of precipitates. Results of material characterization efforts by OSU are planned to be used as inputs to refine model parameters by OSU. The primary purpose for development of the fundamental model is to provided a predictive tool which will assist in more accurate and robust alloying and processing parameter establishment for subsequent phases of the project. A schematic summary of the alloy and process development cycle integrating modeling tools is given in Figure 2.3.1. A high level summary of the OSU model architecture is shown in Figure 2.3.2. Modeling effort under the OSU contract are planned

to continue later than the writing of this report. Additional details concerning the model and results will be available in the OSU final report for this effort.
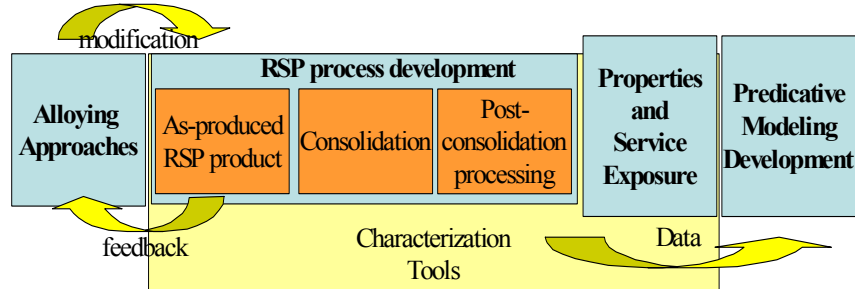

Figure 2.3.1: Schematic of the process for utilization of model results in alloy and process development.
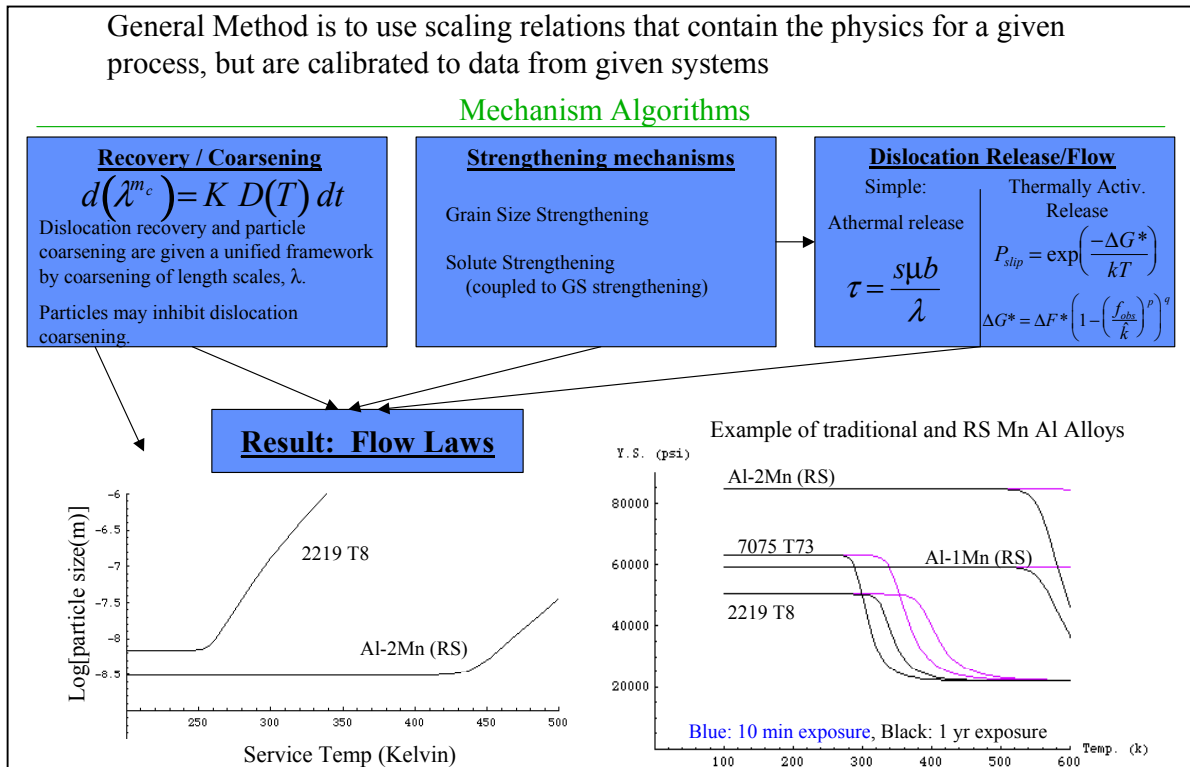

General Method is to use scaling relations that contain the physics for a given process, but are calibrated to data from given systems

Mechanism Algorithms

Recovery / Coarsening

$$d\left(\lambda^{m_c}\right) = K\, D(T)\, dt$$

Dislocation recovery and particle coarsening are given a unified framework by coarsening of length scales, λ.

Particles may inhibit dislocation coarsening.

Strengthening mechanisms

Grain Size Strengthening

Solute Strengthening
(coupled to GS strengthening)

Dislocation Release/Flow

Simple: Thermally Activ. Release

Athermal release

$$\tau = \frac{s\mu b}{\lambda}$$

$$P_{slip} = \exp\left(\frac{-\Delta G^*}{kT}\right)$$

$$\Delta G^* = \Delta F^*\left(1 - \left(\frac{f_{obs}}{\hat{k}}\right)^p\right)^q$$

Result: Flow Laws

Example of traditional and RS Mn Al Alloys

Blue: 10 min exposure, Black: 1 yr exposure

Figure 2.3.1: Summary of the OSU model architecture and early results (bottom right).

III. Technical Summary of the Shape Change Concepts Subtask

This scoping task was performed to establish airfoil geometry shape change requirements based on an aerodynamic assessment and to outline materials approaches and system concepts to meet these shape change requirements. Aerodynamic requirements are primarily establishment of the desired airfoil geometry changes required to maximize specific fuel consumption benefit. Results were used to further define the Phase II plans. Assessment of engine benefits and definition of configuration concepts was performed

using the QAT and GE90 Block 4 engine mission cycles as a baseline. The QAT utilizes a commercial engine cycle with a number of advanced engine technologies studied under other GE Aircraft Engines contract efforts

A. Component Level Concepts for Phase 1 Preliminary Down-Select

Conceptually all compression component airfoils could benefit from shape change capability in order to improve incidence angles and to set more optimum camber levels for off-design conditions. These benefits may result in improved performance, enhanced operability, reduced weight, or a combination of all three. Three application classes were defined to help narrow the focus for concept studies in this effort and to highlight particular differences in how shape changing concepts might be applied. The three classes were:

    1) fan rotor blades
    2) booster and compressor rotor blades
    3) stator vanes and static flowpath surfaces

Fan blades are the most significant airfoil in size and overall impact to engine performance and, therefore, presents the best opportunity to impact fuel burn. Since fan blades must operate over a wide range of conditions, a single blade shape cannot typically represent an optimum geometry for both high power (max climb) and part power (cruise) performance. Rather, fan designs typically compromise performance at both ends of the spectrum to achieve an acceptable single blade shape solution applicable to all cycle conditions. A shape changing fan blade could potentially be tailored such that high power (low camber) and part power (high camber) performance can be optimized. If the fan leading edge (LE) is actuated open at high power, the increase in flow could be used to reduce fan diameter, weight and drag. If the fan LE is actuated closed at cruise, the performance improvement could be used to reduce mission fuel burn significantly.

Booster and compressor blades have a smaller impact on engine performance, but can play a significant role for operability. The intended shape change for these blades would include increased rotor camber at part speed and decreased camber at high speed. Operability enhancements could be converted to lower wheel speeds, smaller diameters, fewer stages, fewer airfoils, or a reduced dependence on variable geometry.

Stator vanes and static flowpath surfaces, such as splitters and bleed ports, define the final class, which generally would have a smaller direct impact on component performance and operability than rotors. Example concepts include actuating a stator LE open or closed to better match incidence, actuating a stator trailing edge (TE) open or closed to control rotor loading, and actuating a splitter to accept variable bypass ratios.

Of the three classes, the fan blade class was chosen for further concept development because it provides a direct linkage to, and potentially the most significant reduction in engine fuel burn. Additionally, the fan blade technical hurdles encountered were envisioned to be somewhat similar to those for booster/compressor rotor components.

B. Fan Airfoil Camber Change Concepts

Airfoil Geometry Change

Figure 3.2.1 illustrates the envisioned camber shape change for the fan airfoil. To increase aerodynamic efficiency, the airfoil adopts its maximum camber for high speed operation at peak power (at take-off through max climb shown in red). At cruise, the blade uncambers for maximum part power performance (blue). A first estimate indicates that a camber change of ~4° at the leading and trailing edges, respectively, provides a fan efficiency cycle performance gain of ~1% over the cruise portion of the entire cycle for a conventional commercial fan engine. The camber is defined as the average between the leading edge and trailing edge metal angles, where the metal angles are measured relative to the rotor axis. A linear increase in the total camber change from 0° at the blade root to 8° at the blade tip was required.

The optimization from take-off to cruise was assumed through an equal (but opposite) change in camber at the leading and trailing edges metal angles. Thus, in order to reduce the total camber of the blade, the trailing edge camber angle would be increased and the leading edge camber angle would be decreased.

Actuation Concepts

Morphing or actuating the blade between the cambered and uncambered states can, in principle, be accomplished in a number of ways, as summarized in Table 3.2.1. Mechanically actuated drives are expected to add unacceptable weight as well as degrading the aerodynamic profile of the airfoils. Piezoelectric & magnetostrictive actuators are limited to approximately 0.1% recoverable strain and require high fields to actuate. In addition, piezoelectric ceramics are brittle and costly to manufacture in any but the simplest shapes. Bimetallic couples, which rely on differences in coefficient of thermal expansion (CTE) to actuate in response to temperature changes, are limited to approximately 0.3% strain (assuming a peak CTE difference of $15\times10^{-6}/°C$ and a limit of 390°F (200°C) on the temperature change) and are subject to non-recoverable plastic deformation (yielding) at strains exceeding this value.
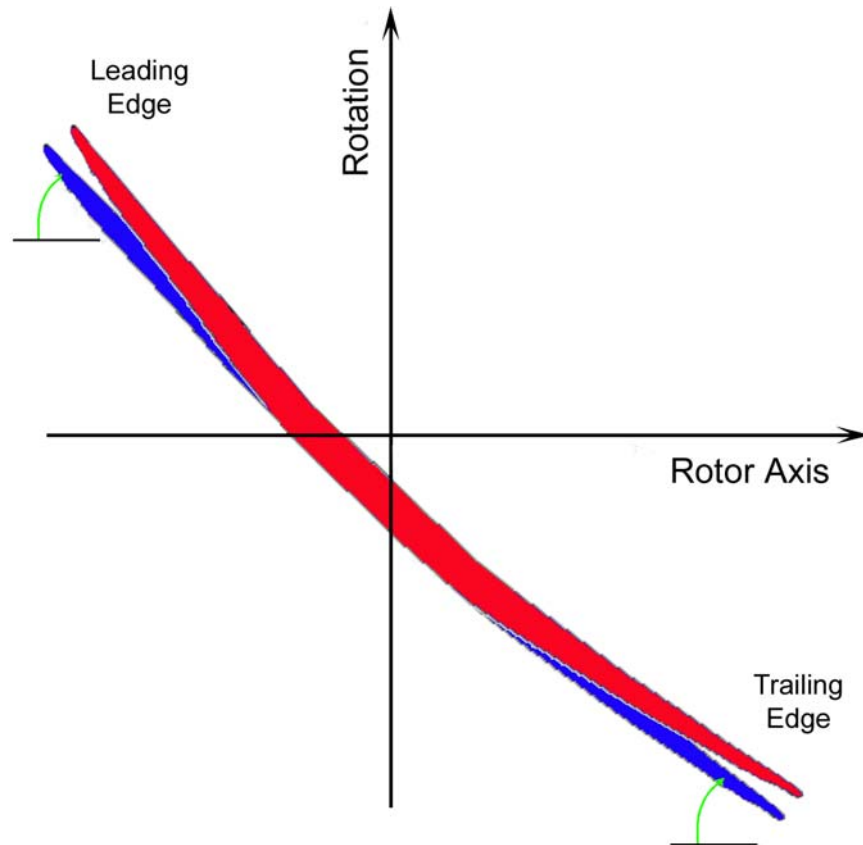
Figure 3.2.1: Leading and trailing edge angles for one blade cross-section.

Table 3.2.1: Comparison of airfoil actuation concepts.

Actuator	Driving Field	Max. Strain [%]	Max. Frequency [kHz]
Mechanical Drive	Mechanical	N/A	0.001
Piezoelectric	Electrical	<0.1	100
Magnetostrictive	Magnetic	<0.1	10
Bimetallic Couple	Thermal	<0.3	0.005
Martensite ⇔ Austenite SMA	Thermal	5-10	0.005
Ferromagnetic SMA	Magnetic	5-10	5

To overcome the above-mentioned shortcomings of the actuation schemes, the airfoil actuation concept examined in this study will utilize the thermally induced shape-memory effect (SME). The mechanism of thermal SME is illustrated in Figure 3.2.2. At its root is a crystallographic phase transformation upon heating or cooling the alloy through the its transformation temperature. This transformation is accompanied by high-strain actuating response. A schematic of the strain response of a shape memory alloy is given in Figure 3.2.3. A number of material systems have been identified and studied which exhibit shape memory behavior over a wide variety of transition temperatures. A summary of some of these systems [9-13] and their actuation temperature ranges are given in Figure 3.2.4. The most common of the shape memory alloy systems is that of Ni-Ti system. Alloy chemistry can be used in many of these systems to controllably affect transition temperature [9,14-15] as shown in Figure 3.2.5.

The airfoil must be actuated between a elastically "relaxed" and "constrained" configurations. The first concept considered was to apply an actuator directly to the airfoil surface. To limit the length of time in the actuated configuration, a blade optimized for cruise performance was chosen as the unactuated state and one optimized for take-off was chosen as the actuated state. A schematic showing the effect of initial "unconstrained" blade shape and placement of the shape memory alloy on the pressure or suction side airfoil surfaces is summarized in Figure 3.2.6.

A number of design requirements and constraints have been identified for the fan airfoil application. The following were used to guide the scoping study:
- Provide desired shape change
- Reversible (e.g., do not exceed recoverable strain limit ANYWHERE on airfoil or actuator)
- Cyclic capability >10,000 actuation events
- Actuation time ~1 minute
- Temperature capability ~50,000 hours at 160°F (71°C)
- Passive actuation (e.g., temperature-induced) or active actuation with a limited instantaneous or average power requirement
- No adverse effects on system (e.g., airfoil fatigue debit, overloading fan disk, loss of aero)
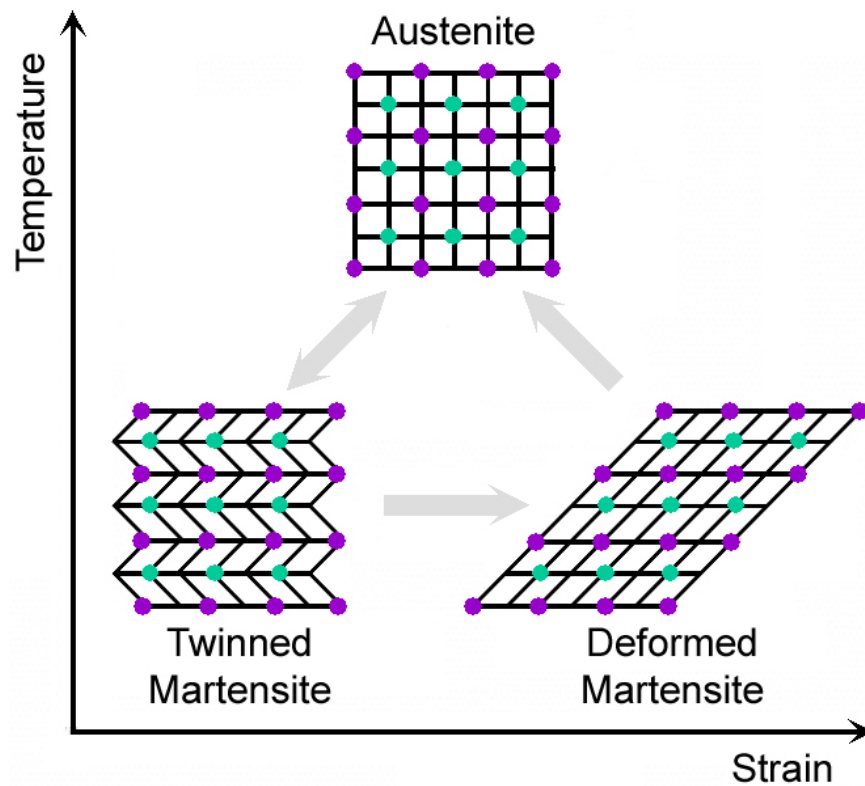- Additional weight < 2 lbs/blade

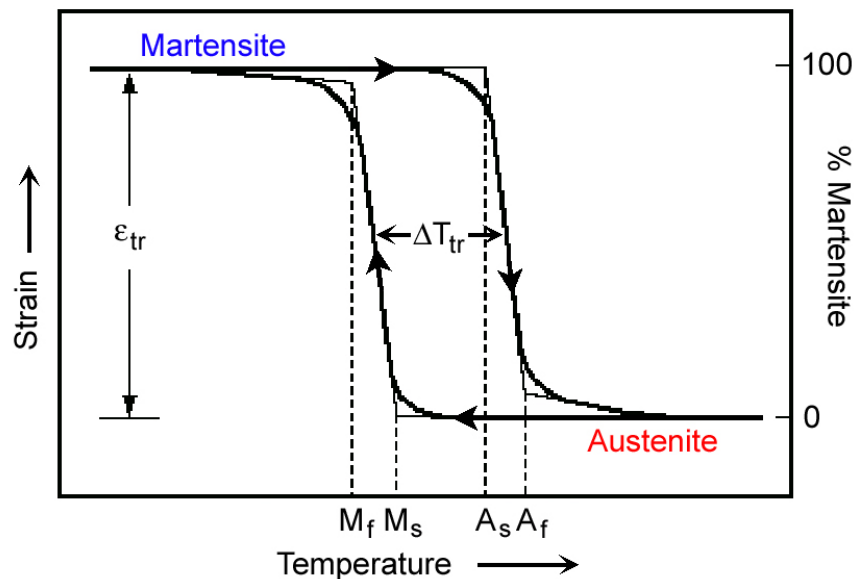Figure 3.2.2: Mechanism of thermal shape memory effect (SME).

Figure 3.2.3: Schematic strain-temperature hysteresis loop for a shape-memory alloy undergoing martensite-to-austenite transformation and subjected to constant load (stress).
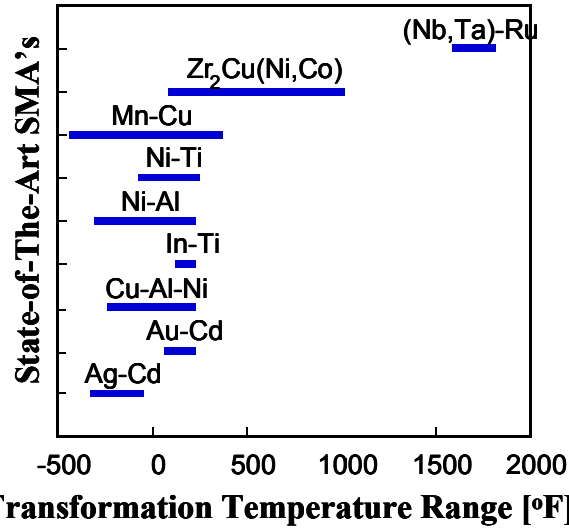
Figure 3.2.4: A summary of typical shape memory alloy transition temperature ranges for various alloy systems [9-13].
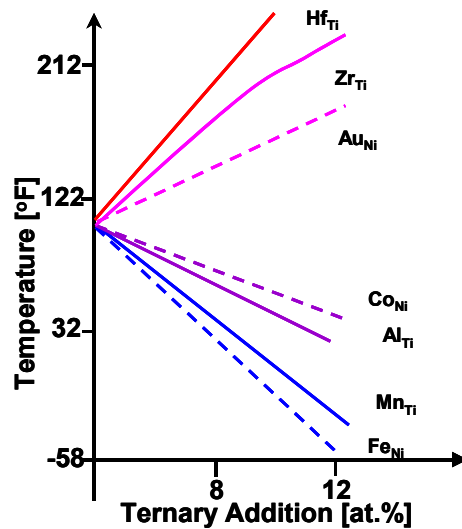

Figure 3.2.5: Effect of alloy composition on Nitinol (Ni-Ti) shape memory alloy transition temperatures [9,14-15]. Note that alloying additions typically substitute for either Ni or Ti in the structure as indicated by the subscripts in the legend.
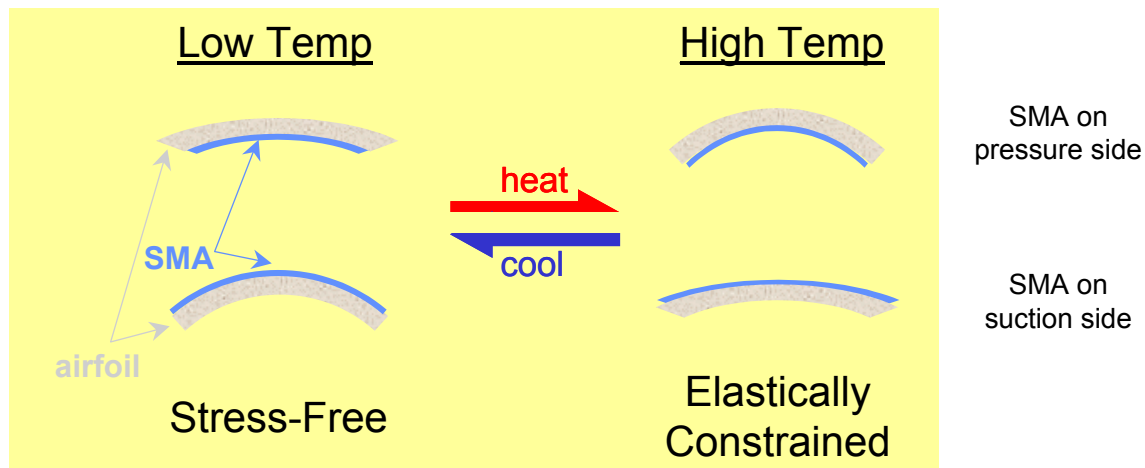
Figure 3.2.6: Schematic of the effect of "unconstrained" airfoil shape and shape memory alloy actuator location on the resulting low and high temperature blade shapes.
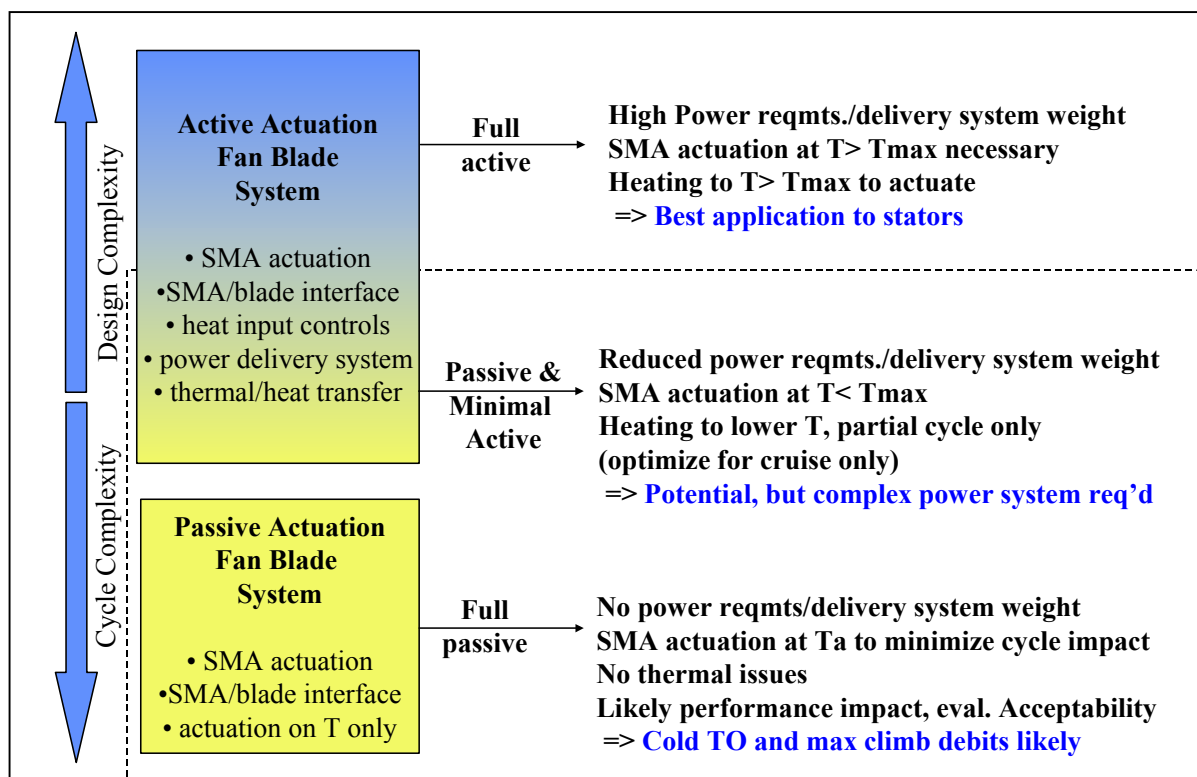
Figure 3.2.7: Summary of potential passive and active shape memory actuation methods.

For a shape memory alloy actuation system, the actuation system design, in its simplest form, would utilize ambient (component) temperature differences during the engine cycle as the driver for actuation. This system would be passive in that no separate control system would be required and no energy inputs would be needed. The use of such a system assumes that the actuated and unactuated airfoil positions correlate directly to distinct temperatures and temperature ranges, and that a shape memory alloy with a

transition temperature lying between these two ranges can be used. Other system configurations including a partially and fully active actuation system could also be considered. These systems, however, would require heating of the shape memory material and an associated power delivery system that would result in both increased electrical power and additional engine weight impacts. A summary of various actuation system concepts is given in Figure 3.2.7. Particularly for a rotating component, it is desirable to utilize passive actuation concepts whenever possible.

During this first phase of the shape change concept study, the actuation concepts and identified shape memory materials systems were considered in assessing the aerodynamic benefit of a shape changing fan blade. Mechanical and thermal analysis was performed based on several candidate configurations in order to assess the viability of overall shape change and actuation configurations on engine performance and efficiency.

C. Analysis of Aero Benefits

The GE90-94B fan blade was used as the baseline geometry to evaluate the performance effect of cambering/uncambering the airfoil. Performance was calculated using GEAE's standard 3D Computational Fluid Dynamics (CFD) Navier-Stokes code, Tacoma, at two operating conditions: mid-cruise near 95% corrected fan speed, and at high power near 105% corrected fan speed. Both cases were run on the cruise operating line using standard day inlet conditions.

Various camber changes were studied to maximize fan efficiency at each condition while maintaining flow at speed. In the spanwise direction, camber changes were distributed linearly tip to hub so that the maximum change occurred at the tip while no change occurred at the hub. In the chordwise direction, the camber distribution was maintained while the magnitude was increased or decreased.

At high-corrected speed, fan efficiency was improved by +1.25 pts by reducing both leading and trailing edge camber by 2 deg (4 deg total) relative to the baseline. At cruise, fan efficiency was improved by 0.72 pts by increasing the leading edge camber by 4 degrees, with no change to the trailing edge. Overall the blade tuned for high speed requires approximately 8 deg less tip camber than the blade tuned for cruise. The linear camber change from tip to hub is crude at best, providing only a rough estimate for the desired camber change. Further inspection of the results suggests that neither "optimum" blade shape had reached its entitlement performance level, and that a more uniform camber change from midspan to the tip would offer further efficiency benefits.

In general, efficiency at high speed can be traded for efficiency at part speed during the design process, and so these results imply that fan performance could be improved by >1 pt across the speed range through well-controlled camber modifications.

GE90 vs QAT

The GE90 blade results were used as the basis to estimate the potential benefit of this technology for a QAT engine cycle. The QAT features a 2-stage counter-rotating fan with suction side bleed on the first stage rotor blade. It was assumed that the shape changing airfoil technology would be applied to rotor 1 only since little benefit could be obtained on rotor 2. Because suction side bleed acts to reduce the suction surface boundary layer loss and shape changing acts primarily to optimize shock position and strength, the two technologies have been assumed to be additive.

For the GE90-94B engine, +1 pt in fan efficiency corresponds to approximately a 13% reduction in entropy generated by the fan blade. Assuming the same 13% entropy reduction for the QAT rotor1 leads to an overall 6.1% entropy reduction for the QAT 2-stage fan component. The resultant net efficiency change for QAT is +0.4 pts. The full efficiency benefit would apply to a fully active actuation system.

Active vs Passive Actuation

Significant barriers such as weight, power requirements, and failure modes made a fully active shape memory actuation system untenable. As a result, the possibility of using passive actuation was studied. GE90-94B mission cycle data was used to determine if an actuation temperature could be defined such that the fan blade would actuate to the high camber position at low corrected speeds and to the low camber position at high-corrected speeds. At corrected speeds below 100%, the fan would benefit from more camber, while at corrected speeds above 100% the fan would benefit from less camber. Most of the mission time is spent in the "cruise leg" region. It was concluded that virtually any actuation temperature selected would result in the wrong blade shape at some operating conditions.

To minimize the power requirement during active actuation of the airfoil, the actuation temperature should be set near 520 R (80°F), with a conventional level of camber as the baseline (un-actuated) geometry. The airfoil would passively actuate and increase in camber below 520 R (80°F) to achieve the cruise performance benefit. However, at climb conditions (high speed at altitude) and on cold day take-offs (high speed at low ambient temperature), the airfoils would require heating to avoid actuating to the high camber, cruise optimized position. The blade surface temperature would need to be increased sufficiently to avoid actuation, but only over a small segment of the mission. Once the fan corrected speed decreased below 100%, the heating could be turned off, and the blade could be allowed to actuate to the high camber position. A fully passive system could be employed only if the penalties at climb and cold day take-off conditions associated with the high camber blades were acceptable.

D. Structural Analysis

Mechanical Analysis

In a first shape memory actuator design, the change in camber was achieved through the contraction of a SMA skin applied over the entire suction surface of the blade. It was assumed that the SMA induced a 0.5% compressive strain during actuation and that the constituents had the properties listed in Table 3.4.1.

Table 3.4.1: Material properties for SMA and titanium blade.

	E (Msi)	ν	κ (BTU/hr-ft-°F)
Blade [17]	16.500	0.33	3.9
SMA [18]	12.375	0.33	10.4

These material properties are consistent with an austenite Nitinol SMA and a titanium fan blade. Actuation was modeled as a free thermal effect in which $\varepsilon_t = \alpha_{SMA}\theta = -0.05$ (θ is a fictitious temperature change) and ε_t for the fan blade is zero. In order to estimate the thickness of the SMA skin necessary to generate the desired camber change, a generalized form of the bimetallic strip solution given in [16] is used. The basic steps in this solution are provided below.

First, it is assumed that two metallic plates of equal length and depth are perfectly adhered along their long axis. Because no external loads are applied each cross section must be in axial and rotational equilibrium.

$$\sum F_x = P_s + P_b = 0$$
$$\therefore P_s = -P_b = P$$
$$\sum M_z = M_s + M_b = \tfrac{1}{2} Ph$$

Here h is the total thickness (h=h_b+h_s). Subscripts *s* and *b* represent the SMA and the fan blade, respectively. Next, it is assumed that each layer must deflect with the same curvature, κ:

$$M_s = E_s I_s \kappa$$
$$M_b = E_b I_b \kappa$$

From the rotational equilibrium equation,

$$\left(E_s I_s + E_b I_b\right)\kappa = \tfrac{1}{2} Ph \, .$$

Finally, a constraint is applied in order to enforce continuity of the deformations across the interface.

$$\varepsilon_t + \frac{P_s}{E_s bh_s} + \tfrac{1}{2}h_s\kappa = \frac{P_b}{E_b bh_b} - \tfrac{1}{2}h_b\kappa$$

Combining the last two equations,

$$\varepsilon_t + h_e\kappa = 0$$

where h_e is an effective thickness and is a function of E_s, E_b, h_s, and h_b. For a total camber change of θ,

$$h_e = \left(\frac{L}{\theta}\right)\varepsilon_t$$

where L is the length. This is a nonlinear equation in terms of the unknown h_s and must be solved iteratively. For the given material properties and a mean blade thickness of 0.37", it was found that a SMA thickness of 0.004" (4 mils) was required. This value was used in a 2D plane strain ANSYS finite element (FE) analysis using 8 node serendipity elements. As shown in Table 3.4.2, the results were in good agreement with the predicted analytical solution. The 0.5° difference between the leading and trailing edge camber change is due to the non-uniform thickness of the blade.

The deformed shaped of the blade is shown in Figures 3.4.1 and Figure 3.4.2. Contours indicate the effective stresses (in psi) and indicate that stresses are well below the blade yield stress.

Table 3.4.2: Predicted (analytical) results and actual (FE analysis) results.

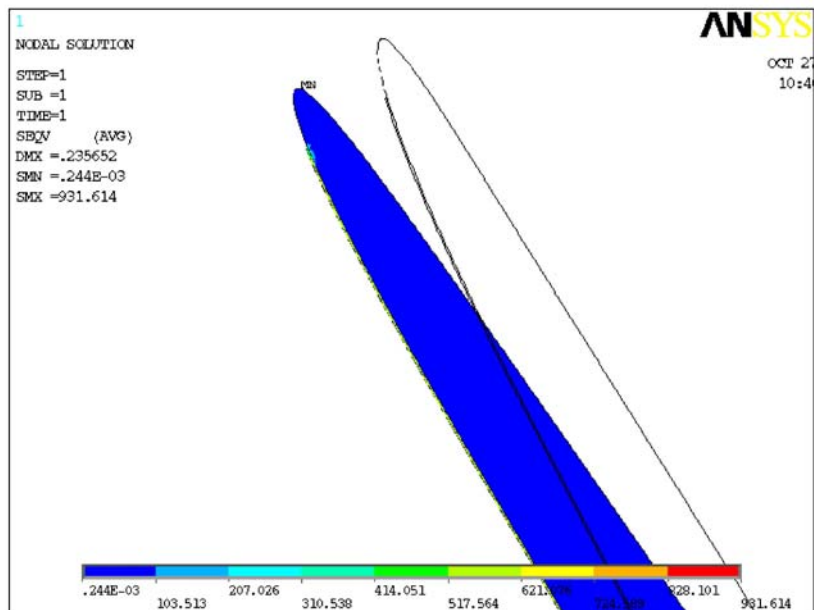|	Desired	Actual
Leading edge camber change	4	3.25
Trailing edge camber change	-4	-3.76
Total camber change	8	7.01

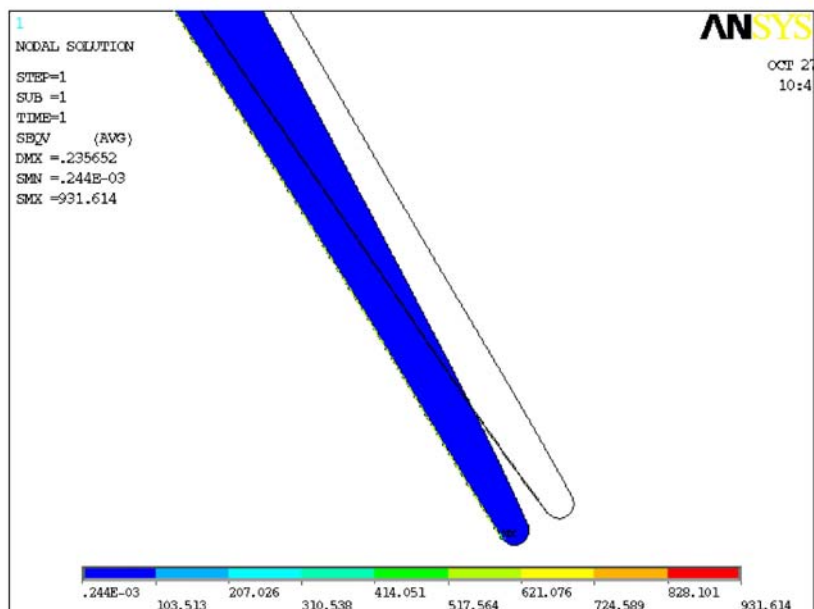Figure 3.4.1: Fan blade leading edge after actuation (color contours) and before actuation (black outline).

Figure 3.4.2: Fan blade trailing edge after actuation (color contours) and before actuation (black outline).

Thermal Analysis

A one-dimensional thermal analysis was performed for this system with convective boundary conditions on the suction and pressure surfaces. The temperature at the SMA-fan blade interface was assumed to be 390°F (200°C), which is approximately the SMA transition temperature. The heat equation was solved for each material and temperature and heat flux continuity was enforced across the interface. The result is three equations in terms of the suction and pressure surface temperatures (θ_1 and θ_2, respectively) and the power required (to maintain the transition temperature in the SMA).

$$\left(\frac{h_s}{2\kappa_s}\right)\left(\frac{\dot{Q}}{bL}\right) - \left(h_s\frac{\beta_s}{\kappa_s} + 1\right)\theta_1 + h_s\frac{\beta_s}{\kappa_s}\theta_o + \theta_{12} = 0$$

$$\left(h_b\frac{\beta_b}{\kappa_b} + 1\right)\theta_2 - h_b\frac{\beta_b}{\kappa_b}\theta_o - \theta_{12} = 0$$

$$\left(\frac{\dot{Q}}{bL}\right) - \beta_s\theta_1 - \beta_b\theta_2 + (\beta_1 + \beta_2)\theta_0 = 0$$

These represent, respectively, the heat equation inside the SMA and inside the blade and the continuity condition at the interface. θ_{12} is the interface temperature (390°F or 200°C) and θ_o is the ambient temperature. The film coefficient (β) for the convective contribution is a function of the apparent velocity (spanwise location) and temperature (altitude) and was assumed to be the same for both surfaces. Two extreme cases were studied: take-off conditions at the blade root (low temperature, low film coefficient) and maximum climb conditions at the blade tip (high temperature, high film coefficient). The input parameters and results are given in Table 3.4.3. The power required is the total for all 22 blades. Results indicate that significant power is required to enable heating of the shape memory material during active actuation periods.

Table 3.4.3. Results of the thermal analysis for take-off and maximum climb [19].

Configuration	β	θ_o	$\dot{Q}$	
	(Btu/ft^2-hr-°F)	(°F)	10^6 Btu/hr	kW
Take-off/blade tip	450	115	10.0	3000
Maximum climb/blade root	35	40	1.7	500

E. Refined Shape Change Airfoil Structure Concept

Titanium blade

To reduce the required power, a second analysis was performed. In this case, thin strips of SMA were placed on the suction surface of the blade at discrete locations along the span. The power required was *assumed a priori* to be 100 kW and the total allowable SMA

width (spanwise) was calculated by linearly scaling the results in Table 3.4.3. This approach is only approximate since it neglects any spanwise heat conduction.

Because convective losses ($\propto$ width) are the major cause of the large power requirement and the camber changes are dependant upon the SMA flexural rigidity ($\propto$ thickness^3), it was proposed that increasing the thickness to width ratio of the strips could substantially reduce the power required. For this reason, two bands of equal width (½") but unequal thickness were used: one 0.005 inches (5 mils) thick placed at the tip and the other 0.0033 inches (3.3 mils) thick placed at the midspan. This provided the desired the blade tip camber change without introducing additional surface area where the convective losses are the greatest.

For the same materials listed in Table 3.4.1, a 3D ANSYS FE analysis using 20 node solid elements was performed. The blade was idealized as a flat plate with a uniform thickness of 0.37 inches. Contours of the vertical (z) displacement are shown in Figure 3.5.1 and the leading/trailing edge camber change as a function of spanwise location is given in Figure 3.5.2.
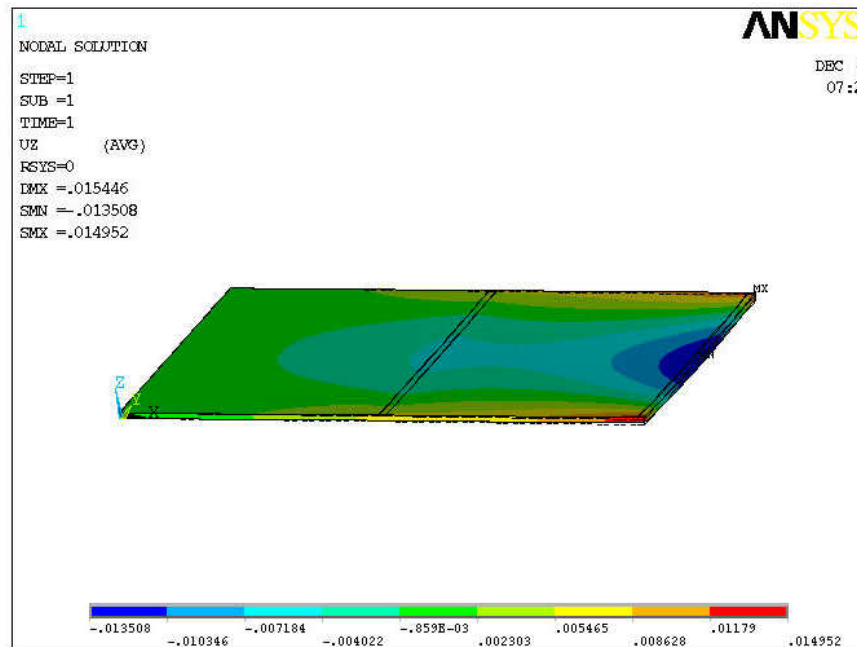

Figure 3.5.1: Contours of the vertical deflection for a two SMA band plate on Ti.
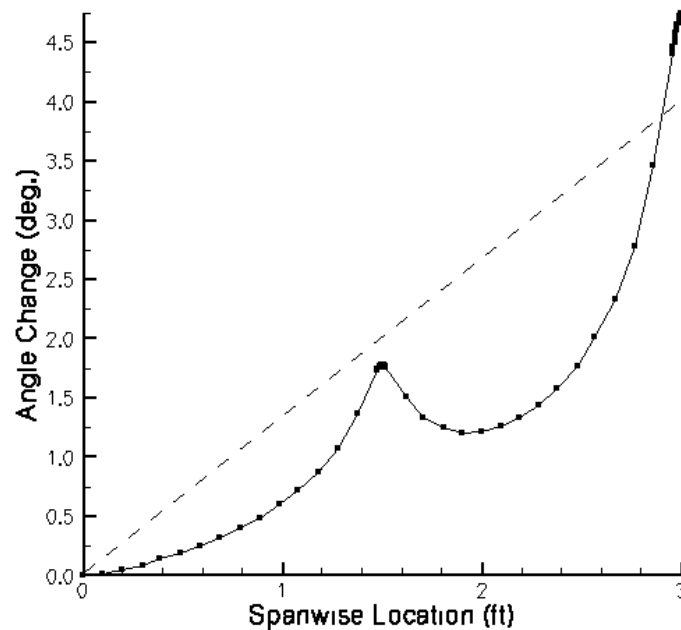
Figure 3.5.2: Variation of the camber change along the span in Ti.

These figures clearly demonstrate that discrete SMA strips can approximate the desired camber change (indicated by the dashed line); however, the result is a nonlinear distribution along the span.

Composite blade

A similar analysis was conducted using the orthotropic properties of a typical composite GE90 fan blade as given below.

In this analysis, four strips of equal width (0.25 inches) were placed at *L/4*, *L/2*, *3L/4*, and *L*. Thus, the total width of SMA material was the same as the previous case. The analytical result predicted a required SMA thickness of 0.002 inches (2 mils) that was used for each strip in the FE model.

Contours of the vertical (z) displacement are shown in Figure 3.5.3 and the leading/trailing edge camber change as a function of spanwise location is given in Figure 3.5.4.
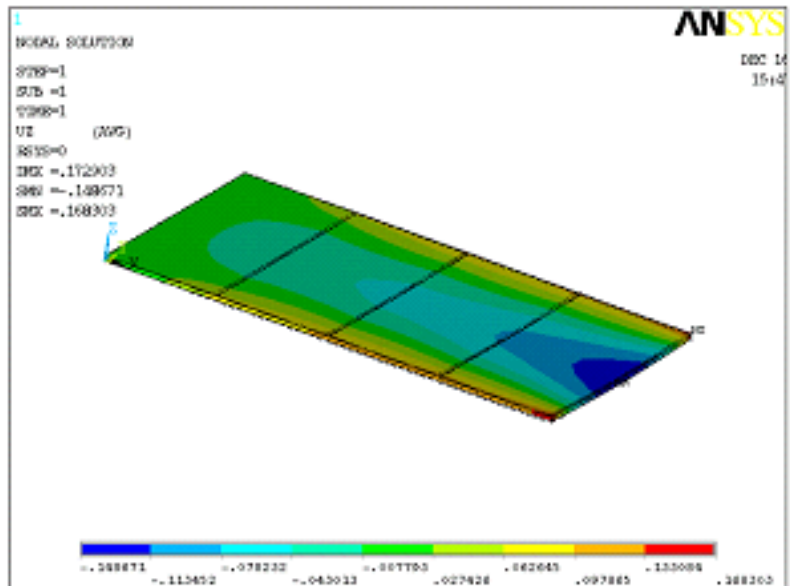
Figure 3.5.3: Contours of the vertical deflection for a two SMA band plate in polymer composite.
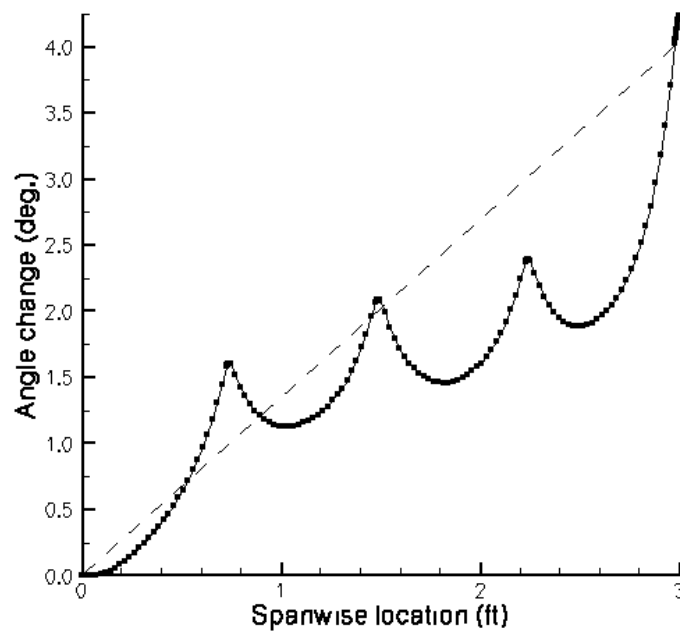

Figure 3.5.4: Variation of the camber change along the span in polymer composite.
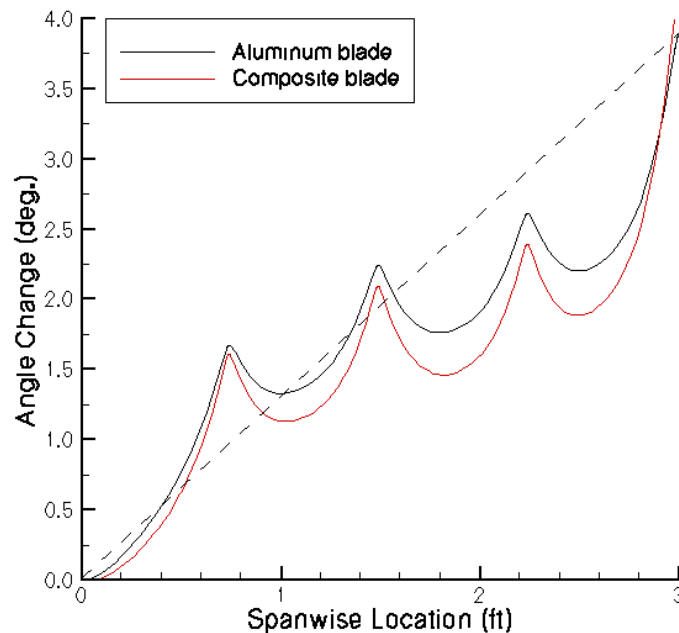
Figure 3.5.5: Comparison of camber changes between the aluminum and composite fan blades.

Again, these figures clearly demonstrate that discrete SMA strips can approximate the desired camber change (indicated by the dashed line). Using more, thinner strips creates a blade shape that is closer to the desired shape over a large span. Because the thickness of these strips is roughly half of that using in the titanium blade, it is likely that the power required in order to maintain the SMA transition would be significantly lower for this configuration.

Aluminum Blade

The four-strip configuration was also studied with a blade comprised of a high strength conventional aluminum alloy 7075 (E = 10.9 Msi, v = 0.33 [20]). Since the elastic modulus of Al 7075 is significantly larger than that of the composite blade, a thicker SMA layer was needed. As predicted by the analytical tool discussed previously, a strip thickness of 0.005 inches (5 mils) was used. The results for the camber change as function of spanwise location are compared to those from the composite blade in Figure 3.5.5.

Again, it is apparent that regardless of the blade material, the desired camber change (indicated by the dashed line) can be achieved through adjustments in the SMA layer.

F. Shape Change System Risk Assessment

Aerodynamic analysis of some first order shape change concepts performed as part of this study suggests that aerodynamic efficiency benefits may be significant if a shape changing

fan blade can be implemented. Several actuation concepts have been considered. Constraints related to consideration of failed mode impact on flight safety and overall power requirements resulted in selection of two shape change airfoil operation methods. A more detailed explanation of the constraints is given subsequently. For both operation methods, the unactuated blade shape was considered to be the nominal baseline QAT blade configuration that is neither optimized for take-off nor cruise. Also, for both methods, the actuated blade shape is that for optimum cruise conditions and actuation would occur when the temperature is below the shape memory alloy transition temperature. The difference in the two methods is that in one, fully passive actuation is assumed whereby the blade temperature is the sole determining factor driving when the blade is in the actuated position and when it is not, whereas, in the other, operation is largely passive with some specific cycle points having active actuation (i.e. heating) to inhibit transition to the actuated optimum cruise blade shape at low temperatures. Specific cycle points which would likely require such partial active actuation include cold day take-off and top of climb cycle points.

From a failure mode perspective, toggling between the optimized for cruise and optimized for high-speed shapes may be unacceptable. If the blade failed in the optimized for cruise position (high camber), performance at high speed would be reduced through almost 2% lower flow and ~3 pts lower efficiency at speed. Such a severe degradation of fan performance would lead to unacceptable impacts on takeoff thrust, EGT, and climb rate. Conversely, if the blade failed in the optimized for high-speed position (low camber), cruise performance would be reduced by more than 1 pt., leading to a substantial fuel burn penalty. Additionally, the low camber position would likely be more prone to aeroelastic instability. A lower risk approach may be to specify the nominal blade shape as the default/primary position, and actuate to the high camber position at cruise to realize the specific fuel consumption (SFC) benefit. An alternate approach could be to specify the nominal blade shape as the default position, and actuate to the low camber position at high corrected speeds for improved temperature and speed margins. For the risk assessment, the nominal, unactuated blade shape was defined as the default QAT baseline blade shape and the actuated shape was defined as the high camber, cruise optimized blade shape.

Assessment of actuation methods has indicated that in the anticipated QAT engine mission cycle, fan blade temperature cannot be exclusively used to permit a passive SMA actuation of the fan blade shape to improve efficiency during cruise. Cold day take-off and top-of-climb mission cycle points present the most difficult issues due to overlap in the anticipated fan blade temperature with that of the cruise condition. Under these two cycle point conditions the take-off blade shape would still be required to meet performance and safety requirements, but the blade temperature would tend to transition the blade shape to the optimum cruise configuration. High level assessment of this and other risks related to passive and active actuation systems have also highlighted concerns related to transients during transition between take-off and cruise blade shapes, complexity and weight of an electrical power delivery system for active SMA actuation, and SMA material transition temperature accuracies anticipated for effective blade shape change.

An assessment of risks associated with each of the two methods – fully active and passive with partially active control - was performed in order to more fully characterize the difficulties and constraints associated with implementation of such a system. A summary is of the top risk items is given in Table 3.6.1. Several risks are common to both the fully passive and the passive/partially active actuation methods. Such risks include uneven actuation of blades when transitioning between actuation states leading to vibration, noise, and loss of performance; overall system complexity and number of failure modes; and the possibility of instantaneous thrust changes when blades are actuated. Risks specific to the fully passive actuation include potential for max climb and cold day take off thrust debits being unacceptable. For the passive/partially active actuation system, the primary risk is that the complex, heavy, power delivery system would be required.

Assessment of the risks associated with the Shape Change Airfoil technology for QAT fan blade applications suggest that there are significant design, performance, safety, and material constraints which would have to be addressed in order to move forward with this technology as it applies to QAT fan blades and the overall QAT mission cycle. It is critical that these issues be assessed to determine the feasibility of implementing such a system.

Table 3.6.1: Summary risk assessment for two shape change fan blade configurations

Passive Actuation with selected Active Actuation
Uneven actuation blade to blade in transition causes vibs, noise, inbalance, other
Power delivery system weight
Power delivery system complexity
Overall System complexity, # fialure modes
Power delivery system requires invention

Full Passive Actuation
Overall System complexity, # fialure modes
FADEC sensing of blade condition (complexity increase)
Instantaneous thrust change and accomodating via engine control
Constraints limit efficiency benefit to point where not viable
Uneven actuation blade to blade in transition causes vibs, noise, inbalance, other
Max climb thrust debit not acceptable, fan dia. increase req'd

G. Implications to the Engine System

The System Study assessment performed as part of the overall GE IPSFT Phase I program examined the overall impact of various technologies to the engine. Inputs to this analysis for this project are summarized in Table 3.7.1. Due to the early stage of development of this technology and several unknowns that had not yet been explored, several assumptions were made to enable an overall assessment. Assumptions are detailed in the table. Resulting performance effects are summarized in Table 3.7.2.

In order to accomplish the shape change, a shape memory alloy strip configuration applied to one surface of the blade was used for the System Study assessment. Only preliminary

assessment of this configuration could be performed under the scope of the Shape Changing Airfoil concept assessment effort and this configuration is not considered to be optimum. Shape memory alloy shape actuation to change the blade shape was assessed and the target configuration assumed that the shape change at cruise could be accomplished in a passive actuation mode using ambient blade temperature transitions to actuate the shape memory material into the cruise condition. However, due to variability in ambient air temperature at take-off and temperatures reached at the top of climb, it was determined that some selected active shape memory alloy actuation would be required to delay blade transition to the cruise condition during a cold day takeoff and during typical top of climb conditions. Several assumptions were used to permit input of data for the system study.

Table 3.7.1: System impact study inputs from the Shape Change Airfoil project.

Parameter	Value	Assumptions
Fan efficiency improvement (ΔED12)	0.40 pt.	Baseline blade shape for unactuated condition, optimized airfoil shape for cruise mission segment.
System Weight	+5 lbs	No consideration of power delivery system weight (if required). Weight increase due to shape memory material added in four bands at ¼ span points and also added resulting impact to stator and disk resulting from increased blade weight.
Electric power requirements	12 hp	Power required only during active actuation portions of engine cycle. Power requirement was spread over the cruise portion of the cycle for simplicity of system modeling.

Table 3.7.2: System study results

Engine Parameter	Estimated Benefit
% Specific fuel consumption	-0.25%
% Fuel burn	-0.25%
% Range	+0.25%

Inputs to the Impact Matrix were made based on the assumptions above and included an assessment of as many of the impacts as was possible from the scope of the Shape Changing Airfoil concept study assessment. A fan efficiency improvement of 0.40 points (ΔED12) was determined based on the ability to modify the baseline QAT blade camber by 4 degrees into the optimum mission cruise stage blade configuration while keeping the standard baseline blade shape under take-off and climb conditions. For the shape memory material configuration, the overall impact to the overall system was 5 pounds versus the baseline QAT when considering additional weight increases in the rotor and stator/containment system resulting from the additional blade weight. No weight impact was taken for any electrical power delivery system required for the active actuation system for cold day take-off and typical top of climb conditions. Assessment of the overall design and corresponding added weight from components needed to route electrical power from

the engine stator through the rotor to the blades was not within the scope of the Shape Changing Airfoil Phase I effort and as a result was considered an unknown. An estimate of the electrical power consumption was included based on power requirements for resistance heating of the shape memory material. Electrical power would only be required during the active actuation portion of the engine cycle, however, for simplicity of system level analysis, the total power requirement was spread over the entire engine cycle yielding a 12 horsepower impact throughout the cycle. Additionally, it was assumed that other factors relating to blade design, power delivery system design, engine performance and safety, formation of a robust mechanical bond between the blade and shape memory material, and robust electrical and thermal isolation of the shape memory material could be accomplished with additional development effort.

Results in Table 3.7.1 indicate that the 0.5% specific fuel consumption goal in this project was not met. Instead a 0.25% benefit was assessed based on a number of significant assumptions.

H. Summary

Scoping of shape changing airfoil concepts including both aerodynamic analysis and materials-related technology assessment effort was performed. Three general categories of potential components were considered – fan blades, booster and compressor blades, and stator airfoils. Based on perceived contributions to improving engine efficiency, the fan blade was chosen as the primary application for a more detailed assessment.   A high-level aerodynamic assessment using a GE90-90B Block 4 engine cycle and fan blade geometry indicates that blade camber changes of approximately +/- 4 degrees would be sufficient to result in fan efficiency improvements nearing 1%. Constraints related to flight safety and failed mode operation suggest that use of the baseline blade shape with actuation to the optimum cruise condition during a portion of the cycle would be likely required. Application of these conditions to the QAT fan blade and engine cycle was estimated to result in an overall fan efficiency gain of 0.4%.

High-level assessment of fan blade operation temperature ranges for critical mission cycle points indicates that passive airfoil shape control using shape memory alloy materials is not likely to be sufficient to trigger shape changes at all of the appropriate points in the engine cycle. Active control mechanisms would likely be required in using shape memory alloy materials in sub-sonic fan blade applications unless expected thrust debits during cold day take-off and max climb portions of the cycle can be accommodated in a passive actuation approach. Structural analysis suggested that actuation strains to achieve desired camber changes could be accomplished with shape memory alloys. Tailoring of the actuated blade shape is possible through variation in the location, shape (thickness, width, length), and the number of discrete SMA patches. However, in order to maximize the enhancement, a thorough mechanical and thermal optimization would still be required.

Assessment of the risks associated with the Shape Change Airfoil technology for QAT fan blade applications suggest that there are significant design, performance, safety, and material constraints which would have to be addressed in order to move forward with this technology as it applies to QAT fan blades and the overall QAT mission cycle. It is critical that these issues be carefully considered if one is to determine the feasibility of implementing such a system.

IV. Conclusions and Recommendations

A. Conclusions based on Phase I study

Based on the Phase I Shape Changing Airfoil project study, the following conclusions were made:

1. Melt spun aluminum flake material can be successfully consolidated to bar by containered extrusion.
2. Rapid solidification techniques such as melt spinning have demonstrated the capability of forming fine microstructures in several aluminum alloys which can be heat treated to yield fine stable particle dispersions if the chemistry permits.
3. Difficulties in introducing aluminum oxide into molten aluminum led to discontinuation of the ceramic dispersion strengthening approach, although characterization did point to the benefits of the Al-Mn system which was pursued further.
4. Al alloy characterization efforts suggested that icosohedral and Al-Mn alloy compositions may be processed to result in fine particle dispersions which are likely to significantly improve strength and temperature capability over conventional high strength 7xxx-series alloys.
5. A Modeling approach developed by OSU focused on linking Al microstructure parameters, deformation conditions and tensile/creep strength. Characterization results will be implemented in the finalized OSU Phase I model used to refine the model.
6. Aerodynamic assessment indicates 0.4% fan efficiency benefit for QAT using a shape changing fan blade concept leading to about a 0.25% specific fuel consumption and 0.25% fuel burn benefit.
7. Mechanical assessment suggests that shape memory alloy materials can be applied to a commercial engine fan blade geometry with a relatively low blade set and overall system weight impact of the order of 5 lbs. Noting that weight associated with a power delivery system had not been assessed and is not included in this estimate.
8. Consideration of active vs. passive control and assessment of system risks indicated significant constraints to both control methods in application to a shape changing fan blade to QAT.

### B. Recommendations based on Phase I Study

Based on the Phase I Shape Changing Airfoil effort the following recommendation are being made.

1. Continued aluminum development, heat treatment, characterization and modeling efforts are recommended in order to enable exploitation of alloying concepts established in this project. Validation of strengthening concepts via mechanical testing is recommended prior to applying strengthening approaches and resulting models to generate more complex alloys.
2. Other applications of this technology to stators and other engine cycles including high Mach flight may be subject to fewer limiting constraints and thus have a more likely path to implementation although the performance impact has not been evaluated in this study. As a result other applications may be more amenable to implementation of these shape change concepts to a stator component. Additional assessment would be required for these other applications.

V. Program Schedule

The Phase I RASER Task Order 23 WE# 3.2 schedule is given in Table 5.1.1 below.

Table 5.1.1: Overall Phase I project schedule
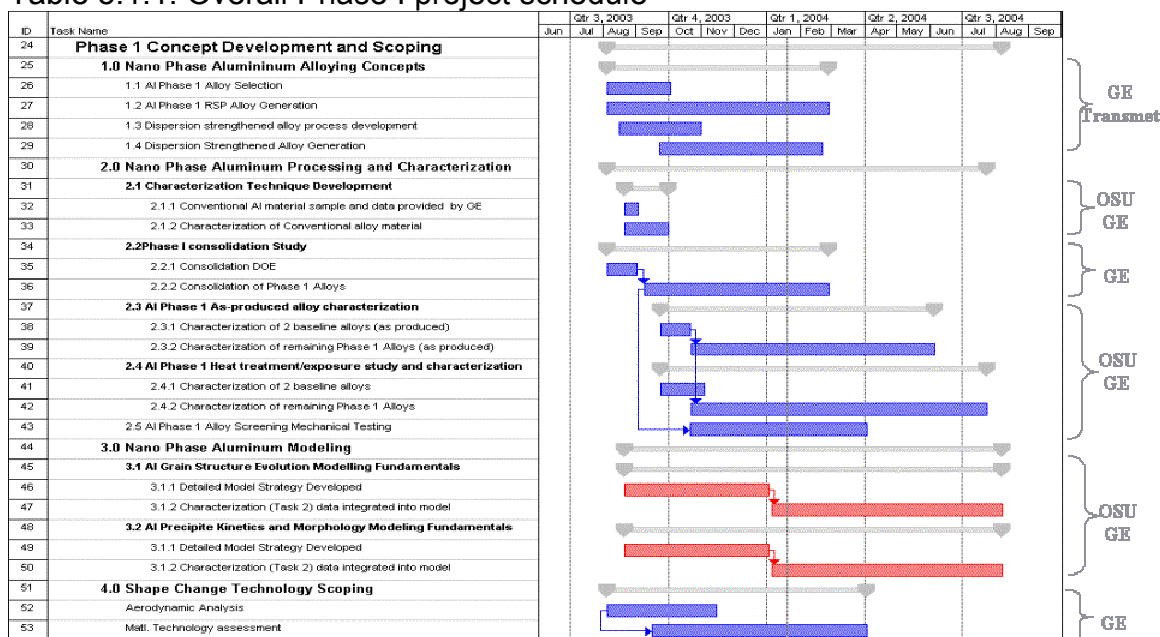
VI. References

1. D. Hull and D.J. Bacon, *Introduction to Dislocations*, International Series on Materials Science and Technology, vol. 37, Pergamon Press, New York, 1984.
2. K. Hiraga, T. Ohsuna, W. Sun and K. Sugiyama, Materials Transactions, vol. 42, 2001, pp.2354-2367.
3. D.J. Skinner, R. L. Rye, D. Raybould and A.M. Brown*, Scripta Metallurgica*, vol. 20, 1986, pp. 867-872.
4. A. Inoue and H. Kimura, in "Aerospace Materials," edited by B. Cantor, H. Assender and P. Grant, published by Institute of Physics Publishing, Bristol, UK, pp. 150-169.

5. A. Inoue and H. Kimura, *Materials Science and Engineering*, vol. A286, 2000, pp. 1-10.

6. K.L. Kendig and D. Miracle, *Acta Materialia*, vol. 50, 2002, pp. 4165-4175.

7. (insert reference for Al-Mn binary phase diagram)

8. T. Koike, H. Yamagata and N. Kanetake, *Journal of Japan Institute of Light Metals*, vol. 51, 2001, pp. 267-272.

9. *Shape Memory Materials* edited by K. Otsuka and C. M.Wayman, Cambridge University Press, 1999.

10. R. Kainuma, H. Nakano, K. Oikawa, K. Ishida and T. Nishizawa, "High Temperature Shape Memory Alloys of Ni-Al Base Systems", *Materials Research Society Symposia Proceedings*, 1992, Vol. 246, pp 403-408.

11. P. L. Potapov, "Martensitic Transformations and High Temperature Shape Memory Effect in the Intermetallic NiMn Alloyed with Ti", *Metal Science and Heat Treatment*, 1993, Vol. 35, No. 9, pp 520-525.

12. G. S. Firstov, J. Van Humbeeck, Yu. N. Koval , "Peculiarities of the martensitic transformation in ZrCu intermetallic compound - potential high temperature SMA" , *Journal de Physique IV*, 2001, Vol. 11, pp 481-486.

13. R. W. Fonda, H. N. Jones and R. A. Vandermeer, "The Shape Memory Effect in Equiatomic TaRu and NbRu Alloys", *Scripta Materialia*, 1998, Vol. 39, No. 8, pp 1031-1037.

14. A.G.Hundzhua, M.I.Zaharova, A.V.Sorokin, "Martensitic Transformation in Alloyed Nickel-Titanium", *Metalphysics*, in Russian, 1986, Vol. 8, No. 2, pp 38-42

15. US Patent 5,114,504 "High Transformation Temperature Shape Memory Alloy", 1992.

16. Timoshenko, S., "Analysis of Bi-Metal Thermostats," *Journal of Applied Mechanics*, v 11, pp. 657-660.

17. Ti-6Al-4V (Grade 5) Material Data Sheet, *ASM (asm.matweb.com)*, 2004.

18. NiTi Material Data Sheet, *Johnson Matthey Inc. (www.sma-inc.com), 2004.*

19. Finn S., Personal communication, *GE Research Center, 2004.*

20. Aluminum 7075 Material Data Sheet, *eFunda* (www.efunda.com), 2004.

REPORT DOCUMENTATION PAGE

Public reporting burden for this collection of information is estimated to average 1 hour per response, including the time for reviewing instructions, searching existing data sources, gathering and maintaining the data needed, and completing and reviewing the collection of information. Send comments regarding this burden estimate or any other aspect of this collection of information, including suggestions for reducing this burden, to Washington Headquarters Services, Directorate for Information Operations and Reports, 1215 Jefferson Davis Highway, Suite 1204, Arlington, VA 22202-4302, and to the Office of Management and Budget, Paperwork Reduction Project (0704-0188), Washington, DC 20503.

1. AGENCY USE ONLY (Leave blank)	2. REPORT DATE October 2005	3. REPORT TYPE AND DATES COVERED Final Contractor Report—July 2, 2003–May 30, 2004

4. TITLE AND SUBTITLE

Shape Changing Airfoil

5. FUNDING NUMBERS

WBS–22–714–92–50
NAS3–01135
Work element 3.2, Task order 23

6. AUTHOR(S)

Eric A. Ott

7. PERFORMING ORGANIZATION NAME(S) AND ADDRESS(ES)

General Electric Aircraft Engines
One Neumann Way
Cincinnati, Ohio 45215–1915

8. PERFORMING ORGANIZATION REPORT NUMBER

E–15289

9. SPONSORING/MONITORING AGENCY NAME(S) AND ADDRESS(ES)

National Aeronautics and Space Administration
Washington, DC 20546–0001

10. SPONSORING/MONITORING AGENCY REPORT NUMBER

NASA CR—2005–213971

11. SUPPLEMENTARY NOTES

Project Manager, Clayton L. Meyers, Aeronautics Division, NASA Glenn Research Center, organization code PRV, 216–433–3882.

12a. DISTRIBUTION/AVAILABILITY STATEMENT

Unclassified - Unlimited
Subject Category: 07

Available electronically at http://gltrs.grc.nasa.gov

This publication is available from the NASA Center for AeroSpace Information, 301–621–0390.

12b. DISTRIBUTION CODE

13. ABSTRACT *(Maximum 200 words)*

Scoping of shape changing airfoil concepts including both aerodynamic analysis and materials-related technology assessment effort was performed. Three general categories of potential components were considered—fan blades, booster and compressor blades, and stator airfoils. Based on perceived contributions to improving engine efficiency, the fan blade was chosen as the primary application for a more detailed assessment. A high-level aerodynamic assessment using a GE90-90B Block 4 engine cycle and fan blade geometry indicates that blade camber changes of approximately $\pm4°$ would be sufficient to result in fan efficiency improvements nearing 1 percent. Constraints related to flight safety and failed mode operation suggest that use of the baseline blade shape with actuation to the optimum cruise condition during a portion of the cycle would be likely required. Application of these conditions to the QAT fan blade and engine cycle was estimated to result in an overall fan efficiency gain of 0.4 percent.

14. SUBJECT TERMS

Propulsion systems (aircraft)

15. NUMBER OF PAGES

50

16. PRICE CODE

17. SECURITY CLASSIFICATION OF REPORT	18. SECURITY CLASSIFICATION OF THIS PAGE	19. SECURITY CLASSIFICATION OF ABSTRACT	20. LIMITATION OF ABSTRACT
Unclassified	Unclassified	Unclassified	